Backward elastic p^3He scattering and structure of the ^{3}He nucleus

Yu. N. Uzikov
Joint Institute for Nuclear Research, Dubna

Fiz. Élem. Chastits At. Yadra **29**, 1010–1052 (July–August 1998)

Mechanisms of backward elastic p^3He scattering at energies of 0.5–2 GeV are studied using the 3- and 4-dimensional nonrelativistic diagrammatic technique. In the first step the structure of the ^{3}He nucleus is described using the approximation of the two-body $d+p$ configuration, and then the three-body 5-channel wave function from solving the Faddeev equations is used. It is shown that the inclusion of the three-particle properties of the ^{3}He structure is crucial. Relativistic effects are taken into account using the relativistic quantum mechanics of systems with fixed numbers of particles, and are found to be unimportant for the dominant mechanism. In addition to mechanisms containing information about the structure of the ^{3}He nucleus at small relative internucleon separations, special attention is paid to the mechanism of sequential np-pair transfer. This mechanism in fact does not require high-momentum components of the nuclear wave functions in spite of the large momentum transfer, and it dominates under certain kinematical conditions. It is shown that when rescattering is taken into account, this mechanism allows the successful description of the available experimental data on the energy and angular dependence of the differential cross section at $\sim 1-2$ GeV without the use of free parameters. The clearly manifested effects due to the $\hat{A}\{(NN)(^1S_0)+N\}$ component of the wave function of the ^{3}He nucleus and Glauber rescatterings in the initial and final states are displayed. The results of a low-energy analysis using the unitarized K-matrix approach are also presented. © *1998 American Institute of Physics.* [S1063-7796(98)00504-X]

1. INTRODUCTION

One of the main problems in the experimental and theoretical study of proton interactions with very light nuclei at large momentum transfer $\Delta > 1$ GeV/c is obtaining information about the structure of these nuclei at small internucleon separations $r_{NN} \sim 1/\Delta \sim 0.5$ F and about the NN interaction in the nucleon overlap region. Such information is valuable, as it can be directly related to fundamental problems in the theory of strong interactions: color confinement and quark–hadron duality, and it is impossible in principle to obtain it from processes with small momentum transfer. In pd collisions the simplest process with large momentum transfer is backward elastic pd scattering. In this process the deuteron makes full use of its ability to elastically absorb, as a whole, a large momentum and energy transfer a hundred times greater than its binding energy. Theoretical analyses have systematically studied the question of the degree to which this property of the deuteron can be related to the 6-quark and relativistic structure of its wave function. In another elastic process, p^3He backward scattering at initial energies of 1–2 GeV, large momentum transfers $\Delta \sim 3$ GeV/c are attained[1] which significantly exceed those in electron scattering.[2] This allows us to hope that it will be possible to obtain new information about the structure of the ^{3}He nucleus from this process for small NN separations which is not available from e^3He scattering.

The active study of backward elastic pd scattering over the last three decades has given rise to a number of interesting ideas in intermediate-energy physics, like the existence of nucleon isobars N^* in nuclei[3] and three-baryon resonances.[4] The important role of virtual pions has been revealed,[5,6] and the question of the color dynamics in this process has been posed.[7] Obvious progress has been made in describing backward elastic p^3He scattering at energies 0.5–1 GeV (Ref. 8) and 1–1.7 GeV (Refs. 9 and 10). However, it should be realized that, given the current state of the theory of these processes, they do not represent a sufficiently refined tool for studying the high-momentum components of the deuteron and ^{3}He wave functions. It is now becoming more and more clear that the relation between the observed characteristics and the nuclear wave function is not obvious even for the simplest mechanisms, neutron exchange in $pd \to dp$ processes or np-pair exchange in $p^3\text{He} \to {}^3\text{He}p$ processes, owing to effects of the initial- and final-state interactions, the role of which is quite important despite the high collision energy.[9,11,12] In addition, it has been shown that at certain energies a large momentum transfer can occur, owing to mechanisms which do not significantly involve the high-momentum components of the nuclear wave function. In backward pd scattering one such mechanism is double pN scattering with Δ-isobar excitation, which dominates at initial energies in the range 0.5–1.0 GeV. A more refined example of the masking of the nuclear structure at short distances in reactions with large momentum transfer is that of backward elastic p^3He scattering. In this process at $T_p = 1-2$ GeV and $\theta_{\text{c.m.}} = 180°$ the insensitivity to the high-momentum components of the nuclear wave function is not related to the excitation of nucleon resonances, but instead is a consequence of the specific three-body structure of the ^{3}He nucleus.

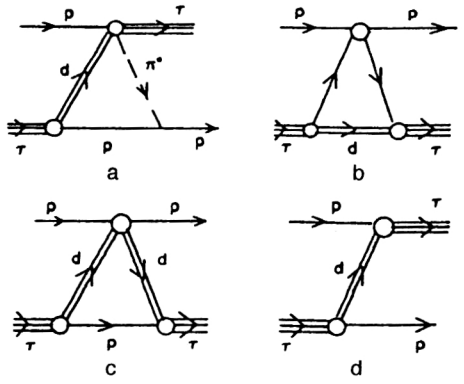

FIG. 1. Mechanisms for backward elastic p^3He scattering with the $d+p$ configuration for the ^{3}He nucleus. (a) One-pion exchange (OPE); (b) single scattering on a virtual proton (SS); (c) single scattering on a virtual deuteron (SSVD); (d) deuteron exchange (DE).

In this review we discuss the results obtained in recent years on the theoretical analysis of the process $p^3\text{He} \to {}^3\text{He}p$. We present a critical analysis of the studies in which attempts are made to describe backward elastic p^3He scattering on the basis of a simplified picture of the interaction involving only the $^3\text{He} \leftrightarrow d+p$ vertex, neglecting rescattering. We present the results of a more systematic description of this process obtained using the three-body wave function of the ^{3}He nucleus on the basis of the diagrammatic and operator formalisms for the scattering amplitude, taking into account the initial- and final-state interactions. The results of the analysis show that in backward elastic p^3He scattering the effects of the initial- and final-state interactions, and also nuclear-structure effects, are manifested more clearly than in the $pd \to dp$ process. Therefore, in the opinion of this author, backward elastic p^3He scattering in the range 1–2 GeV is at present better understood than backward elastic pd scattering, in spite of the fact that the ^{3}He nucleus is a more complicated object than the deuteron.

2. THE $d+p$ APPROXIMATION FOR THE ^{3}He WAVE FUNCTION

The literature contains several models for the process $p^3\text{He} \to {}^3\text{He}p$, proposed on the basis of analogy with backward elastic pd scattering (see Fig. 1): the triangle graph of one-pion exchange (OPE) with the subprocess $pd \to {}^3\text{He}\pi^0$ (Refs. 1 and 13), heavy-particle stripping,[14,15] and the microscopic optical model including antisymmetrization of the pN amplitudes.[8] The deuteron-transfer mechanism was studied in Ref. 10 using relativistic light-cone dynamics. The common features of these models are the following: high sensitivity of the calculated characteristics to the structure of the ^{3}He nucleus at small NN separations, and a completely satisfactory description of the experimental data on the scattering cross section at angles close to $\theta_{\text{c.m.}} = 180°$. However, this agreement is obtained under assumptions about the structure of the ^{3}He nucleus which are too greatly simplified, and the initial- and final-state interactions are neglected. In the present review we begin our analysis of backward elastic p^3He scattering by analyzing such models restricted to the $d+p$ configuration of the ^{3}He nucleus, and we compare the predictions with the results obtained using the three-body ^{3}He wave function.

In this section we display the role of the $d+p$ configuration of the ^{3}He nucleus in backward elastic p^3He scattering at 400–1700 MeV, using the mechanisms of deuteron exchange and single pp and pd scattering, and the mechanism with the subprocess $pd \to {}^3\text{He}\pi^0$. We also present the results of calculating the charge form factor of the ^{3}He nucleus using the approximation $^3\text{He} = d+p$.

2.1. The charge form factor of ^{3}He in the $d+p$ approximation

In restricting ourselves to the $p+d$ configuration of ^{3}He, all the matrix elements of processes occurring on ^{3}He are expressed in terms of the overlap integral of the three-body wave function of ^{3}He, $\psi_\tau^{\sigma_\tau}$, and the product of the deuteron wave function $\psi_d^{\sigma_d}$ and the proton wave function $\chi_{1/2}^{\sigma_p}$:

$$G(\rho) = \langle \chi_{1/2}^{\sigma_p} \psi_d^{\sigma_d}(\mathbf{r}) | \psi_\tau^{\sigma_\tau}(\mathbf{r},\rho) \rangle$$
$$= \sum_{L=0,2,M,S,\sigma} \left(LMS\sigma \middle| \frac{1}{2}\sigma_\tau \right) \times \left(1\sigma_d \frac{1}{2}\sigma_p \middle| S\sigma \right) U_L(\rho) Y_{LM}(\hat{\rho}), \quad (1)$$

where $S=3/2$ for $L=2$ and $S=1/2$ for $L=0$. Here we have used the standard notation for the spherical harmonics Y_{LM} and the Clebsch–Gordan coefficients. The S and D components of the wave function $U_L(\rho)$ given by (1) were found in Ref. 16 from the solution of the Faddeev equations with the Reid soft-core potential for the NN interaction. Here we use these results with the following normalization condition for the wave functions U_0 and U_2:

$$\int_0^\infty [U_0^2(\rho) + U_2^2(\rho)] \rho^2 d\rho = 1. \quad (2)$$

Actually, the three-body calculations give a value less than unity, 0.43 [Ref. 17], for the normalization integral (2). However, it can be hoped that the normalization (2) effectively includes the contribution of the configuration $p+d^*$ with the pn pair in the singlet state. We parametrize the wave functions $U_0(r)$ and $U_2(r)$ as

$$U_0(r) = \sum_{i=1}^{5} \alpha_i \exp(-\beta_i r^2),$$
$$U_2(r) = \sum_{i=1}^{5} \delta_i r^2 \exp(-\gamma_i r^2). \quad (3)$$

The coefficients of the expansions in (3) are given in Table I.

To determine the values of the momentum transfer for which this two-body approximation is reasonable, we calculate the charge form factor F_{ch}^τ of ^{3}He with the wave functions of Ref. 16. Restricting ourselves to the $p+d$ configuration in the ^{3}He wave function, we obtain the following expression for the charge form factor:

TABLE I. Coefficients of the expansion.

α_i, F$^{-3/2}$	β_i, F^{-2}	δ_i, F$^{-7/2}$	γ_i, F^{-2}
1.80112 E−02	2.15766 E−02	−1.93862 E−03	9.83826 E−02
2.13255 E−01	8.35379 E−02	−1.58838 E−02	3.18527 E−01
9.00237 E−02	1.27578 E−01	−3.11061 E−02	6.43963 E−01
3.23190 E−01	3.26778 E−01	−3.83184 E−02	1.19183 E+00
−2.17017 E−01	1.06206 E+00	−9.57312 E−02	4.47721 E+00

$$F_{\rm ch}^{^3{\rm He}}(\Delta)=\frac{1}{2}F_{\rm ch}^{p}(\Delta)\left\{F_{000}\left(\frac{2}{3}\Delta\right)+F_{022}\left(\frac{2}{3}\Delta\right)\right\}$$
$$+\frac{1}{2}[F_{\rm ch}^{p}(\Delta)+F_{\rm ch}^{n}(\Delta)]\left\{S_s^d\left(\frac{1}{2}\Delta\right)\times\left[F_{000}\left(\frac{1}{3}\Delta\right)+F_{022}\left(\frac{1}{3}\Delta\right)\right]\right.$$
$$\left.+\frac{1}{\sqrt{8\pi}}S_Q^d\left(\frac{1}{2}\Delta\right)\left[\sqrt{8}F_{220}\left(\frac{1}{3}\Delta\right)-F_{222}\left(\frac{1}{3}\Delta\right)\right]\right\}. \quad (4)$$

Here Δ is the momentum transfer, and $S_s^d(\Delta)$ and $S_Q^d(\Delta)$ are the scalar and quadrupole form factors of the deuteron from Ref. 18. The form factors $F_{lLL'}$ are defined below by Eq. (15). For the nucleon form factor $F_{\rm ch}^N(\Delta)$ we use the parametrization of Ref. 19.

The results of the calculation are compared with the experimental data[20] in Fig. 2. For $\Delta\leq 1.5$ GeV/c the calculation using (4) does not differ significantly from that using the impulse approximation with the three-body wave function of the ^{3}He nucleus for the Reid soft-core potential.[21] However,

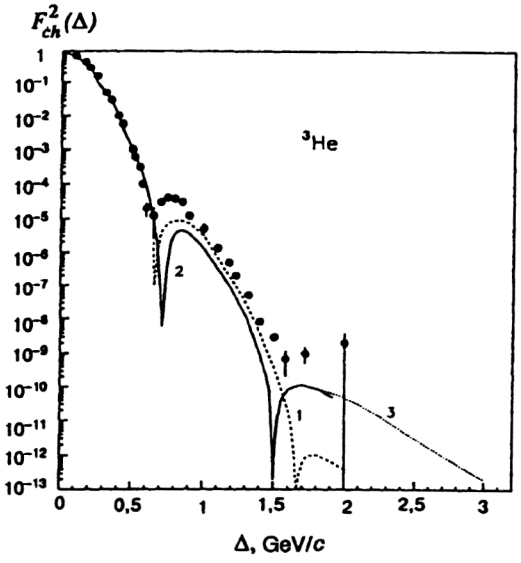

FIG. 2. Results of calculating the ^{3}He charge form factor in the impulse approximation: (1) including only the $d+p$ configuration; (2) using the three-body wave function of the ^{3}He nucleus (Ref. 16) for the Reid soft-core potential; (3) extrapolation of the form factor to momentum transfers $\Delta=2-3$ GeV/c. The points (●) are the experimental data of Ref. 20.

for $\Delta\geq 1.5$ GeV/c it is already clear that the high-momentum component in the $p+d$ configuration has insufficient weight, which causes the curve calculated in the two-body approximation to lie considerably lower than the curve obtained for the three-body wave function. It can therefore be concluded that the $p+d$ configuration corresponding to Eqs. (1) and (2) dominates in the ^{3}He charge form factor for momentum transfers $\Delta\leq 1.5$ GeV/c. For $\Delta\sim 1.5$ GeV/c the experimental data are not accurate enough to confirm the existence or precisely determine the location of the second theoretical minimum of the charge form factor.

2.2. Mechanisms for backward elastic p^3He scattering restricted to the $p+d$ configuration of ^{3}He

2.2.1. The potential approach

In potential theory the amplitude of elastic p^3He scattering taking into account the Pauli principle can be written as two terms:

$$\langle f|\tau|i\rangle=\langle f|\tau_{\rm MS}|i\rangle-\langle f|\tau_{\rm ex}|i\rangle. \quad (5)$$

Here $\tau_{\rm MS}$ is the modified multiple-scattering series, and the operator $\tau_{\rm ex}$ describes the exchange of a two-nucleon cluster accompanied by pN rescattering. In earlier studies[15–22] it has been shown that it is possible to describe backward elastic p^4He scattering by using the $p+t$ configuration for the ^{4}He nucleus. A similar approach to describing backward p^3He scattering limited to the $p+d$ configuration has been taken in Ref. 23. Let us briefly describe the results of Ref. 23.

In the Born approximation the first term in (5) reduces to the sum of graphs for single scattering (SS) on the proton and single scattering on the virtual deuteron (SSVD). The second term coincides with the pole graph for deuteron exchange (DE; see Fig. 1). In the case of unpolarized particles, for the differential cross section given by the sum of these graphs we obtain

$$\frac{d\sigma}{d\Omega_{\rm c.m.}}=\frac{1}{4\pi^2}\left(\frac{E_pE_\tau}{E_p+E_\tau}\right)^2[\overline{|M_{\rm DE}|^2}+\overline{|M_\Delta|^2}+\overline{M_{\rm DE}M_\Delta^*}+\overline{M_{\rm DE}^*M_\Delta}]. \quad (6)$$

Here $M_{\rm DE}$ is the deuteron-exchange amplitude, M_Δ is the sum of the SS and SSVD amplitudes, and E_p and E_τ are the total energies of the proton and the target nucleus.

After averaging and summing over spins, for the squared modulus of the amplitude $M_{\rm DE}$ we find

$$\overline{|M_{\rm DE}|^2}=\frac{16\pi^2}{3}N_{pd}^2\left(\frac{p_d^2-m_d^2}{2m_d}\right)^2\left\{[U_0^2(q)+U_2^2(q)]^2+4\left[U_0(q)U_2(q)+\frac{1}{\sqrt{8}}U_2^2(q)\right]^2P_2(\mathbf{qq}')\right\}, \quad (7)$$

where N_{pd} is a combinatorial factor equal to 2, corresponding to the two protons of the target nucleus; $p_d^2=(p_\tau-p_p)^2$ is the squared 4-momentum of the virtual deuteron; and q and q' are the relative 3-momenta at the $\tau\to d+p$ and

$d+p\to\tau$ vertices. According to relativistic quantum mechanics,[24] for the momenta $\mathbf{q}$ and $\mathbf{q}'$ we have

$$\mathbf{q}=\frac{\varepsilon_p+E_p}{E_p+E_d+M_{pd}}\,\mathbf{p}'_\tau-\mathbf{p}_p,$$

$$\mathbf{q}'=-\frac{\varepsilon_p+E_p}{E_p+E_d+M_{pd}}\,\mathbf{p}_\tau-\mathbf{p}'_p, \tag{8}$$

$$\varepsilon_p=\sqrt{q^2+m_p^2},\quad E_j=\sqrt{m_j^2+\mathbf{p}_j^2}, \tag{9}$$

where $\mathbf{p}_j$ is the momentum of the jth particle in the $p+\tau$ c.m. frame; M_{pd} is the invariant mass of the $p+d$ system,

$$M_{pd}^2=\{\sqrt{m_p^2+Q_0^2}+\sqrt{m_d^2+2Q_0^2(1+\cos\Theta_{\text{c.m.}})}\}^2-Q_0^2; \tag{10}$$

and $\mathbf{Q}_0$ is the relative momentum in the $p+{}^3$He system.

After averaging and summing over spins, we find the following expressions for $\overline{|M_\Delta|^2}$ and $\overline{M_\Delta^* M_{\text{DE}}}$:

$$\overline{|M_\Delta|^2}=N_{pd}^2|A_{pp}+A_{pd}|^2; \tag{11}$$

$$\overline{M_\Delta^* M_{\text{DE}}}+\overline{M_\Delta M_{\text{DE}}^*}=\frac{4\pi}{3}N_{pd}^2\frac{p_d^2-m_d^2}{2m_d}2\text{Re}(A_{pp}+A_{pd}); \tag{12}$$

$$A_{pp}=t_{pp}(\Delta)\left\{F_{000}\left(\frac{2}{3}\Delta\right)+F_{022}\left(\frac{2}{3}\Delta\right)\right\}; \tag{13}$$

$$A_{pd}=(t_{pp}+t_{pn})\left\{S_s^d\left(\frac{1}{2}\Delta\right)\left[F_{000}\left(\frac{1}{3}\Delta\right)+F_{022}\left(\frac{1}{3}\Delta\right)\right]+\frac{1}{\sqrt{8\pi}}S_Q^d\left(\frac{1}{2}\Delta\right)\left[F_{220}\left(\frac{1}{3}\Delta\right)-F_{222}\left(\frac{1}{3}\Delta\right)\right]\right\}; \tag{14}$$

$$F_{lLL'}(\Delta)=\int_0^\infty j_l(\Delta\rho)U_L(\rho)U_{L'}(\rho)\rho^2d\rho. \tag{15}$$

Here $\Delta=\mathbf{p}'_\tau-\mathbf{p}_\tau$ is the momentum transferred in the process $p{}^3\text{He}\to{}^3\text{He}p$, and $S_s^d(\Delta)$ and $S_Q^d(\Delta)$ are the scalar and quadrupole form factors of the deuteron taken from Ref. 18. Equations (11)–(14) involve the t matrix of elastic pN scattering, t_{pN}; here we include only the scalar part and use the usual Gaussian parametrization.

For large momentum transfer the target proton is far from the mass shell, and so the impulse approximation is not applicable for the amplitude t_{pN}. Here for the numerical calculations we use the so-called optimal approximation,[25] in which binding effects and the Fermi motion of the proton in the target nucleus are taken into account. As a result, the amplitude $t_{pp}(T_{\text{eff}},\Delta)$ is taken to be on-shell not at the proton lab energy, but at some effective energy whose value depends on the momentum transfer. We note that owing to the Pauli principle, the amplitude t_{pp} contains two terms: a direct term and an exchange term, with the exchange term dominating in backward scattering.

2.2.2. The OPE mechanism

The one-pion exchange mechanism (see Fig. 1a) with the subprocess $p+d\to{}^3\text{He}+\pi^0$ does not arise in the purely potential approach because it is associated with the production of new particles. Here we shall describe backward $p{}^3$He scattering on the basis of the OPE mechanism, using a formalism analogous to that of Ref. 6 for pd scattering, and one analogous to that of Ref. 26 for $p{}^4$He scattering. The cross section for the process $p{}^3\text{He}\to{}^3\text{He}p$ in the c.m. frame is expressed in terms of the cross section for the process $p+d\to{}^3\text{He}+\pi^0$ on the mass shell as

$$\left(\frac{d\sigma}{d\Omega}\right)_\theta^{p\tau\to\tau p}=\frac{3}{4}\frac{G^2}{4\pi}F^2(k_\pi^2)\frac{T_p+2m_p}{(m_p+T_p)^2}\frac{s_{pd}}{s_{p\tau}}\frac{|q_{pd}|}{|q_{\pi\tau}|}\frac{m_\tau}{m_d}\times\{I_0^2(\kappa,\tilde{p})+I_2^2(\kappa,\tilde{p})\}\left(\frac{d\sigma}{d\Omega}\right)_\Phi^{pd\to\tau+\pi^0} \tag{16}$$

The parameters used here, $T_p, k_\pi, \tilde{p}, \kappa, s_{ij}, |q_{ij}|$, the π-meson form factor $F(k^2)$, and also the relation between the angles θ and Φ are also found in Refs. 6 and 26, and $G^2/4\pi=14.7$. The dependence of the OPE amplitude on the spatial part of the ^{3}He wave function in the S- and D-wave channels of ${}^3\text{He}\to d+p$ scattering is contained in the integrals I_0 and I_2:

$$I_L(\kappa,\tilde{p})=\int_0^\infty j_1(\tilde{p}\rho)(\kappa\rho+1)\exp(-\kappa\rho)U_L(\rho)d\rho, \tag{17}$$

where j_1 is the first-order spherical Bessel function. Owing to the factor $\exp(-\kappa\rho)$ (where $\kappa=0.7-1.0$ F^{-1}), in the energy range of interest 0.4–1.7 GeV the integral (17) is determined by the average value of the function $U_L(\rho)$ in the range $0\leq\rho\leq\kappa^{-1}$. It should be noted that the integral (17), in contrast to the form factors (15) and the Fourier components $U_L(q)$, is not very sensitive to the high-momentum components of the target-nucleus wave function. The experimental data on the cross section for the process $pd\to\tau\pi^0$ at $\Phi_{\text{c.m.}}=180°$ are taken from Ref. 1, and the parameters of the pN scattering amplitude are from Ref. 27.

2.2.3. Comparison with experiment

In Fig. 3 we compare the calculated cross section with the experimental data. Two distinct features of the cross section for $p{}^3$He scattering at $\theta_{\text{c.m.}}=180°$ are observed experimentally: a kink at $\sim$0.5 GeV and a shoulder in the range 1.0–1.5 GeV. In Ref. 1 the OPE model[13] was used to relate these two features to the appearance of the corresponding Δ-resonance singularities of the process $pd\to{}^3\text{He}\pi^+$. However, as can be seen from Fig. 3, the cross section in the OPE model only corresponds in shape to the experimental cross section at energies 0.5–1.3 GeV; the magnitude of the calculated value is almost an order of magnitude lower than the experimental data. The same conclusion follows from Ref. 13. We have calculated the cross section using Eq. (4.13) from Ref. 13 with the data of Ref. 1 on the $pd\to{}^3\text{He}\pi^+$ reaction and the value $U_0(0)=0.42$ F$^{-1/2}$ (Ref. 16) used in Ref. 1. The resulting curve coincided to within a few percent with the OPE curve in Fig. 3 (curve 1) calculated using Eqs. (16) and (17). Therefore, the OPE graph does not explain the experimental data, which means that other mechanisms must be more important.

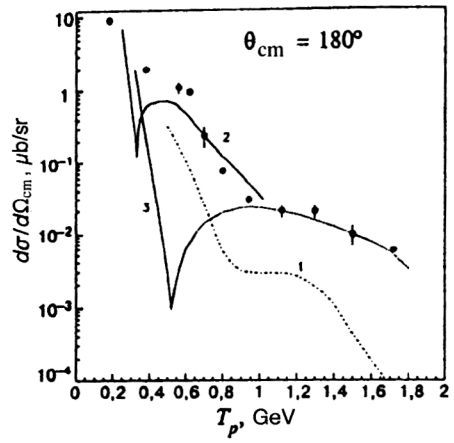

FIG. 3. Calculated differential cross section for elastic p^3He scattering at the angle $\theta_{c.m.}=180°$ as a function of the initial proton energy. (1) OPE; (2) DE; (3) SS using the extrapolation of the ^{3}He form factor from curve 3 of Fig. 2. The points (●) are the experimental data of Ref. 1.

According to the results of the description of the charge form factor of ^{3}He, the contribution of the SS and SSVD single-scattering mechanisms, estimated for the $d+p$ component of the nuclear wave function, can be compared to experiment only for momentum transfers $\Delta\leqslant 1.5$ GeV/c, i.e., for proton energies below 0.55 GeV. Calculation shows that the contribution of the SSVD mechanism is negligible compared to that of the SS mechanism. Near the minimum of the SS amplitude the contribution of the DE pole graph is quite significant, owing to the D-wave contribution. The shoulder predicted by the DE mechanism qualitatively corresponds to the kink observed experimentally. At energies in the range 0.5–1.0 GeV the contribution of the DE mechanism decreases rapidly, while the contribution of single pN scattering grows. Using the estimate for the SS amplitude $M_{pN}=f_{pp}\times F(\Delta)$, where $F(\Delta)=F_{\rm ch}^{\rm theor}/(F^p+\frac{1}{2}F^n)$ is the elastic form factor extracted from the theoretical charge form factor $F^{\rm theor}$ (Ref. 21), we find that the cross section for single pN scattering at 0.9 GeV corresponds in magnitude to the experimental value. This result agrees with the basic conclusion of Ref. 8, where the backward p^3He scattering process was studied at energies $T_p\leqslant 1.0$ GeV. Assuming that the SS mechanism dominates at $T_p=1-1.7$ GeV/c, the elastic ^{3}He form factor at $\Delta=2-3$ GeV/c can be extracted from the experimental data. The corresponding charge form factor is shown by the dotted line in Fig. 2. The behavior of the angular dependence of the cross section is consistent with this assumption.[23]

It would therefore appear that the main goal of our analysis, that of obtaining "new information" about the structure of the ^{3}He nucleus, has been achieved. That is, we have estimated the elastic form factor in the transfer range $\Delta=2-3$ GeV/c inaccessible from electron data. Similarly, the authors of Ref. 10 analyzed the same experimental data and concluded that it is possible to obtain the momentum distribution in the channels $^3\text{He}\to d+p$ and $^3\text{He}\to d^*+p$ at large relative $d-p$ and d^*-p momenta from backward elastic p^3He scattering. However, more careful analysis based on the use of the complete three-body wave function of the ^{3}He nucleus taking into account the initial- and final-state interactions shows that these conclusions are premature, and that the mechanism of backward p^3He scattering at energies $T_p=1-1.7$ GeV is much more complicated.

3. THE AMPLITUDE FOR *np*-PAIR TRANSFER IN THE PROCESS $4+\{123\}\to 1+\{423\}$ IN THE 4-DIMENSIONAL DIAGRAMMATIC TECHNIQUE

The main defect of Refs. 13–15, where the heavy-particle stripping mechanism was studied, is the use of phenomenological two-body wave functions of the ^{3}He nucleus restricted to the $d+p$ configuration, assuming that the weight S_{pd} of this configuration is equal to unity. Even if the overlap integral between realistic deuteron and ^{3}He wave functions, which satisfactorily describes the ^{3}He charge form factor for momentum transfers $\Delta\leqslant 1.5$ GeV/c, is used, the results of analyzing the process $p^3\text{He}\to{}^3\text{He}p$ cannot be considered self-consistent. First, the assumption $S_{pd}=1$ contradicts the results of the three-body calculations,[17] where $S_{pd}=0.43$, and thus overestimates the contribution of the deuteron-exchange mechanism by a factor of 0.43^{-2}. Second, the stripping of a heavy fragment is reduced exclusively to the deuteron-exchange mechanism. The contribution of the singlet deuteron d^* to the d^*+p configuration of the ^{3}He nucleus is included in Ref. 10. However, the author of that study actually uses only the two-body approximation and, moreover, neglects the initial- and final-state interactions. Meanwhile, calculations using the three-body wave function of ^{3}He at low energies[28] show that the contribution of the mechanism of noninteracting np-pair transfer to backward elastic p^3He scattering is comparable to the contribution of deuteron exchange and increases with increasing energy. The contribution of two-stage $n-p$ transfer is found to dominate even in reactions of the type (p,t) for intermediate nuclei at energies $T_p\leqslant 50$ MeV (Ref. 29).

A detailed analysis of the np-pair transfer mechanism based on the loop graphs of the nonrelativistic 4-dimensional diagrammatic technique[33] was performed in Refs. 9, 28, 30–32. The relation between this formalism and the 3-dimensional diagrammatic technique and the Schrödinger formalism was studied. The Faddeev 5-channel wave function including the S and D components was used to describe the structure of the ^{3}He nucleus. The contribution of relativistic effects was estimated. The initial- and final-state interactions were included using the Glauber–Sitenko multiple-scattering theory. The results of this analysis show that the noninteracting-pair transfer mechanism gives the dominant contribution to the np-transfer amplitude at scattering angles $\theta_{c.m.}\sim 180°$. The contribution of deuteron transfer, the amplitude of which is very sensitive to the high-momentum components of the ^{3}He wave function, is negligible. On the other hand, one of the interesting and unexpected features of the dominant mechanism is its weak sensitivity to the structure of the ^{3}He nucleus at small NN separations.

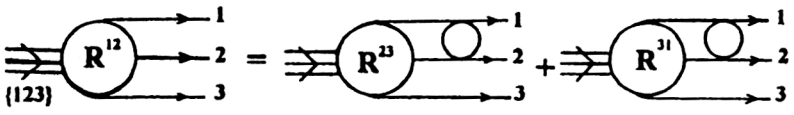

FIG. 4. Equations for the amplitudes R^{ij}.

3.1. The amplitude of virtual decay of the three-particle bound state {123}→1+2+3

We shall start from the technique of nonrelativistic Feynman diagrams.[33] Looking ahead, we remark that the dominant mechanism is insensitive to relativistic effects. This makes the use of the nonrelativistic technique more justified. In processes involving ^{3}He (^{3}H) nuclei, the central feature of the diagrammatic approach is the amplitude of virtual decay of the three-particle bound state {123} into three nucleons: {123}→1+2+3. The quantity with the simplest analytical properties is the cut-off part of this amplitude $R^{ij}(\mathbf{q}_{ij},\mathbf{Q}_k,E_{ij})$, which is the sum of only those graphs which terminate in the interaction between particles with indices i and j. Here $\mathbf{q}_{ij}$ and E_{ij} are the momentum and energy of the relative motion in the pair ij, and $\mathbf{Q}_k$ is the momentum of the spectator nucleon k in the c.m. frame of the nucleus $\{ijk\}$. For arbitrary masses of the particles i, j, and k we have

$$\mathbf{q}_{ij}=(m_j\mathbf{p}_i-m_i\mathbf{p}_j)/(m_i+m_j),$$

$$E_{ij}=E_i+E_j-(\mathbf{p}_i+\mathbf{p}_j)^2/2(m_i+m_j),$$

$$\mathbf{Q}_{k;ij}=[(m_i+m_j)\mathbf{p}_k-m_k(\mathbf{p}_i+\mathbf{p}_j)]/(m_i+m_j+m_k), \quad (18)$$

where E_i and $\mathbf{p}_i$ are the kinetic energy and momentum of the ith nucleon in an arbitrary reference frame. The amplitude R^{ij} is a function of four independent Galilean invariants and satisfies the system of integral equations represented graphically in Fig. 4.

The solution of this system can be written as (to simplify the notation, here and below we do not write out the spin indices or spin functions of the nucleons)

$$R^{12}(\mathbf{q}_{12},\mathbf{Q}_3,E_{12})=\int \frac{d^3q}{(2\pi)^3}\frac{t_{12}(\mathbf{q},\mathbf{q}_{12},E_{12})}{\mathbf{q}^2/2\mu_{12}-E_{12}-i\epsilon}\times L_{12}(\mathbf{q},\mathbf{Q}_3)\{\psi^{23}(\mathbf{q}'_{23},\mathbf{Q}'_1)+\psi^{31}(\mathbf{q}'_{31},\mathbf{Q}'_2)\}, \quad (19)$$

where

$$L_{ij}(\mathbf{q}_{ij},\mathbf{Q}_k)=\mathbf{q}_{ij}^2/2\mu_{ij}+\mathbf{Q}_k^2/2\mu_k+\varepsilon; \quad (20)$$

ε is the binding energy of the three-particle system, $\mu_{ij}=m_im_j/(m_i+m_j)$, $\mu_k=m_k(m_i+m_j)/(m_i+m_j+m_k)$; $\psi^{ij}(\mathbf{q}_{ij},\mathbf{Q}_k)$ is the Faddeev component of the wave function of the nucleus $\{ijk\}$ satisfying the Faddeev equations[34]

$$L_{ij}(\mathbf{q}_{ij},\mathbf{Q}_k)\psi^{ij}(\mathbf{q}_{ij},\mathbf{Q}_k)=-(2\pi)^3\int d^3q'_{ij}t_{ij}(\mathbf{q}_{ij},\mathbf{q}'_{ij},E_{ij}=-\varepsilon-\mathbf{Q}_k^2/3\mu_k)\{\psi^{ki}(\mathbf{q}'_{ki},\mathbf{Q}'_j)+\psi^{jk}(\mathbf{q}'_{jk},\mathbf{Q}'_i)\}. \quad (21)$$

The Jacobi momenta $\mathbf{q}'_{ki},\mathbf{Q}'_k$ and $\mathbf{q}'_{jk},\mathbf{Q}'_i$ differ from the corresponding unprimed variables expressed in terms of $\mathbf{q}_{ij}$ and $\mathbf{Q}_k$ by the replacement $\mathbf{q}_{ij}\to\mathbf{q}'_{ij}$.

Equation (19) is valid in general when the initial nucleus is on the mass shell and all three final nucleons are off-shell, i.e., $\sigma_i\neq 0$, $\sigma_j\neq 0$, and $\sigma_k\neq 0$, where

$$\sigma_i=E_i-\mathbf{p}_i^2/2m_i. \quad (22)$$

In particular, if the kth nucleon is on-shell ($\sigma_k=0$), Eq. (19) for R^{ij} is considerably simplified and in this case we use the special notation Γ^{ij} for it:

$$\Gamma^{ij}(\mathbf{q}_{ij},\mathbf{Q}_k)\equiv R^{ij}(\mathbf{q}_{ij},\mathbf{Q}_k,E_{ij}=-\varepsilon-\mathbf{Q}_k^2/2\mu_k)=-L_{ij}(\mathbf{q}_{ij},\mathbf{Q}_k)\psi^{ij}(\mathbf{q}_{ij},\mathbf{Q}_k). \quad (23)$$

In deriving (23) from (19) we have used the kinematical identity

$$E_{ij}+\sigma_k=-\varepsilon-\mathbf{Q}_k^2/2\mu_k, \quad (24)$$

owing to which the denominator in the integrand of (19) takes the form

$$\mathbf{q}^2/2\mu_{12}-E_{12}=\mathbf{q}^2/2\mu_{12}+\mathbf{Q}_3^2/2\mu_3+\varepsilon=L_{12}(\mathbf{q},\mathbf{Q}_3); \quad (25)$$

then we used Eq. (21).

Finally, let us give the expression for the total breakup amplitudes R, Γ, and also for the full bound-state wave function ψ_A:

$$R=R^{12}+R^{23}+R^{31};$$

$$\Gamma=\Gamma^{12}+\Gamma^{23}+\Gamma^{31};$$

$$\psi_A=\psi^{12}+\psi^{23}+\psi^{31}. \quad (26)$$

The individual components R^{ij} and ψ^{ij} are obtained from (19) and (21) by cyclic permutation of the indices i, j, and k.

3.1.1. The loop diagram of np-pair transfer in the 4-dimensional diagrammatic formalism

Let us consider the transfer of a pair of nucleons 2 and 3 in the reaction $4+\{123\}\to 1+\{423\}$, setting $m_i=m_j=m_k=m$, where m is the nucleon mass. Here we first assume that all the nucleons are nonidentical, and later on we separately take into account the fact that they are identical. Neglecting rescattering in the initial, final, and intermediate states, the most general expression for the two-nucleon transfer amplitude is given by the sum of graphs in Fig. 5. The graphs of Figs. 5a and 5b respectively correspond to the transfer of a pair of noninteracting and a pair of interacting nucleons numbered 2 and 3. We stress the fact that the lower vertex ($R'_i=R_i^{12}+R_i^{31}$) and the upper vertex ($R'_f=R_f^{42}+R_f^{34}$) of these graphs do not contain the amplitude R^{23}. The graph in Fig. 5b can be simplified if the equations for R^{ij} (see Fig. 4) are used to associate the amplitude t_{23} with the upper or

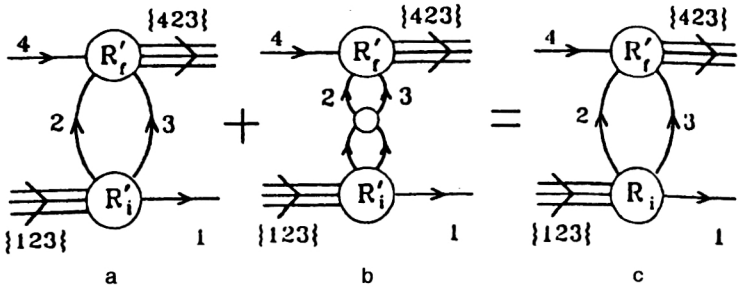

FIG. 5. Two-particle transfer amplitude for the process $4+\{123\} \to 1+\{423\}$ in terms of the 4-dimensional diagrammatic technique: (a) noninteracting-pair transfer (NIPT); (b) interacting-pair transfer (IPT); (c) the total two-particle transfer amplitude. $R_i' = R_i^{12}+R_i^{31}$ and $R_f' = R_f^{42}+R_f^{34}$.

lower vertex. Using one of these possibilities (for example, the second), we obtain the graphical equation shown in Fig. 5.

The analytic expression for the total amplitude (Fig. 5c) has the form

$$M = \frac{i}{(2\pi)^4}\int d^3p_3 dE_2 (R_f^{24}+R_f^{34})(R_i^{12}+R_i^{23}+R_i^{31}) \times (E_2-\mathbf{p}_2^2/2m+i\eta)^{-1}(E_3-\mathbf{p}_3^2/2m+i\eta)^{-1}. \quad (27)$$

We note that Eq. (27) can be rewritten by replacing $(R_f^{24}+R_f^{34})(R_i^{12}+R_i^{23}+R_i^{31})$ by $(R_f^{23}+R_f^{24}+R_f^{34}) \times (R_i^{12}+R_i^{31})$. In both versions the component R^{23} appears only in one of the vertices of the graph in Fig. 5c, and so the double counting of the terms of the multiple-scattering series corresponding to this process is eliminated.

We analyze the features of the integrand in (27) in the complex E_2 plane, using the energy conservation law in the lower vertices of the graphs in Fig. 5:

$$E_2+E_3 = \frac{\mathbf{p}^2}{2m_\tau} - \frac{\mathbf{p}'^2}{2m} - \varepsilon, \quad (28)$$

where $\mathbf{p}$ ($\mathbf{p}'$) is the momentum of the initial (final) proton in the $p+{}^3$He c.m. frame and m_τ is the mass of the ^{3}He nucleus. We take into account the fact that the amplitude $R^{ij}(\mathbf{q}_{ij},\mathbf{Q}_k,E_{ij})$ has a right-hand cut in the E_{ij} plane running from 0 to ∞ with physical values on its upper edge and poles for $E_{ij}<0$ shifted into the lower half-plane and corresponding to bound states in the $\{ij\}$ system.[33] From this, using (18) and (19), we deduce the following regarding the integrand in (27):

1. $R_f^{24}R_i^{23}$ and $R_f^{24}R_i^{12}$ have a right-hand cut and poles in the lower E_2 half-plane;
2. $R_f^{34}R_i^{23}$ and $R_f^{34}R_i^{31}$ have a left-hand cut and poles in the upper E_2 half-plane;
3. $R_f^{34}R_i^{12}$ and $R_f^{24}R_i^{31}$ have both right- and left-hand cuts, and the upper and lower edges of these cuts, respectively, are physical.

3.2.2. The interacting-pair and nonsequential pair transfer mechanisms

In cases 1 and 2 we can integrate over E_2 in (27), taking the residues at the poles $E_2 = \mathbf{p}_2^2/2m_2 - i\eta$ and $E_3 = \mathbf{p}_3^2/2m_3 - i\eta$, respectively. As a result we obtain

$$M_{\rm IPT} = \int \frac{d^3\mathbf{p}_2}{(2\pi)^3}\left(\frac{\Gamma_f^{34}\Gamma_i^{23}}{\tilde\sigma_3}+\frac{\Gamma_f^{24}\Gamma_i^{23}}{\tilde\sigma_2}\right) \quad (29)$$

for $R_f^{34}R_i^{23}+R_f^{24}R_i^{23}$ and

$$M_{\rm NPT} = \int \frac{d^3p_2}{(2\pi)^3}\left(\frac{\Gamma_f^{24}\Gamma_i^{12}}{\tilde\sigma_2}+\frac{\Gamma_f^{34}\Gamma_i^{31}}{\tilde\sigma_3}\right) \quad (30)$$

for $R_f^{34}R_i^{31}+R_f^{24}R_i^{12}$, where

$$\tilde\sigma_3 = \sigma_3|_{\sigma_2=0}, \quad \tilde\sigma_2 = \sigma_2|_{\sigma_3=0}.$$

Taking into account energy and 3-momentum conservation at each vertex of the graphs in Fig. 5, after simple algebra we find

$$\sigma_2 = \tilde\sigma_3 = -(\varepsilon+\mathbf{q}_{23}^2/2\mu_{23}+\mathbf{Q}_{1;23}^2/2\mu_{1;23}) = -L_{23}(\mathbf{q}_{23},\mathbf{Q}_{1;23}). \quad (31)$$

Therefore, using (23), we have

$$M_{\rm IPT} = -(2\pi)^3\int d^3p_2(\psi_f^{24}+\psi_f^{34})^+\psi_i^{23}L_{23}(\mathbf{q}_{23},\mathbf{Q}_{1;23}), \quad (32)$$

$$M_{\rm NPT} = -(2\pi)^3\int d^3p_2(\psi_f^{24^+}\psi_i^{12} + \psi_f^{34^+}\psi_i^{31})L_{23}(\mathbf{q}_{23},\mathbf{Q}_{1;23}). \quad (33)$$

It should be noted that the amplitude $M_{\rm IPT}$ is the exact analytic expression for the interacting-pair transfer (IPT) mechanism (Fig. 5b). The amplitude $M_{\rm NPT}$ is the sum of one-loop graphs with coupling of the vertices $R_f^{24}R_i^{12}$ and $R_f^{34}R_i^{31}$. Using Eq. (19) and Fig. 4, it is easily shown that graphs of this type can be represented in an equivalent "three-loop" form, as shown in Fig. 6. (This result is completely obvious from the graphical equation shown in Fig. 4.) For this reason, we shall refer to the amplitude $M_{\rm NPT}$ as the nonsequential pair transfer (NPT) mechanism.

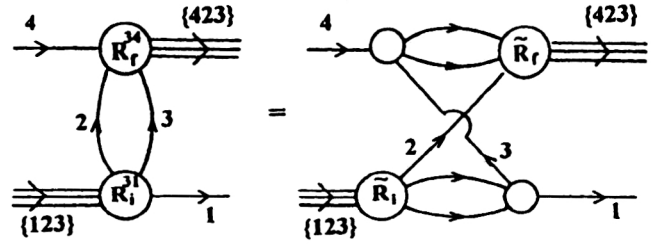

FIG. 6. Four-dimensional graph for nonsequential pair transfer (NPT). $\tilde R_i = R_i^{23}+R_i^{12}$, $\tilde R_f = R_i^{23}+R_f^{42}$.

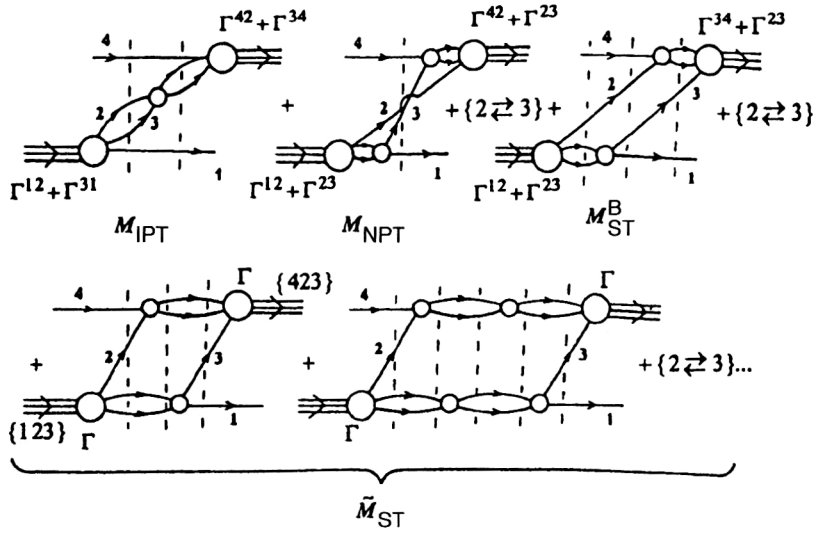

FIG. 7. Three-dimensional amplitudes $M_{\rm IPT}$, $M_{\rm NPT}$, and $M_{\rm ST}=M^{\rm B}_{\rm ST}+\tilde{M}_{\rm ST}$, given by Eqs. (37), (38), (40), and (41). The vertical lines denote the free 4-particle Green function (35). The vertex functions Γ^{ij} and Γ are given by (23) and (26), respectively.

3.3.3. The sequential transfer mechanism

The remaining terms in (28) corresponding to case 3 of the above classification of singularities are grouped into the following expression:

$$M_3=\frac{i}{(2\pi)^4}\int d^3p_2dE_2\,\frac{R_f^{34}R_i^{12}+R_f^{24}R_i^{31}}{(\sigma_2+i\eta)(\sigma_3+i\eta)}. \tag{34}$$

It is impossible to integrate explicitly over E_2 in Eq. (34) by the method of residues. Nevertheless, the amplitude (34) can also be represented in the form of multiple integrals over 3-momenta,[32] which in turn are expressed as an infinite sum of 3-dimensional graphs.

The resulting expression does not contain the energies E_{ij} as independent variables, but is determined by only the 3-momenta. Therefore, in what follows the corresponding amplitude, like (32) and (33), is interpreted within the 3-dimensional diagrammatic technique.

3.2. The *np*-transfer amplitude in the 3-dimensional representation

In the 3-dimensional diagrammatic technique all intermediate particles and their bound states are on-shell, and the basic quantities are the 3-dimensional vertex functions Γ^{ij} (23), the operators t_{ij}, and the four-particle Green function G_0:

$$G_0=(\tilde{\mathscr{E}}_i-\tilde{\mathscr{E}}+i\eta)^{-1}, \tag{35}$$

where $\tilde{\mathscr{E}}_i$ ($\tilde{\mathscr{E}}$) is the total energy of the initial (intermediate) state of the system of four nucleons, taking into account their rest masses. For example, for the $4+\{123\}\to 1+2+3+4$ transition without change of the momentum of nucleon 4 we have ($|\mathbf{p}_4|=|\mathbf{p}_\tau|=|\mathbf{p}|$)

$$\begin{aligned}G_0&=\left[m_4+\frac{\mathbf{p}_4^2}{2m_4}+m_\tau+\frac{\mathbf{p}_\tau^2}{2m_\tau}-\sum_{i=1}^{4}\left(m_i+\frac{\mathbf{p}_i^2}{2m_i}\right)\right]^{-1}\\&=-L_{23}^{-1}(\mathbf{q}_{23},\mathbf{Q}_{1;23})=-L_{31}^{-1}(\mathbf{q}_{31},\mathbf{Q}_{2;31})\\&=-L_{12}^{-1}(\mathbf{q}_{12},\mathbf{Q}_{3;12}).\end{aligned} \tag{36}$$

Now Eqs. (32) and (33) in abbreviated notation take the form

$$M_{\rm IPT}=(\Gamma_f^{24}+\Gamma_f^{34})G_0\Gamma_i^{23}, \tag{37}$$

$$M_{\rm NPT}=\Gamma_f^{24}G_0\Gamma_i^{12}+\Gamma_f^{34})G_0\Gamma_i^{31}, \tag{38}$$

and the amplitude $M_{\rm ST}$ can be written as

$$M_{\rm ST}=M^{\rm B}_{\rm ST}+\tilde{M}_{\rm ST}, \tag{39}$$

$$M^{\rm B}_{\rm ST}=\Gamma_f^{34}G_0\Gamma_i^{12}+\{2\leftrightarrow 3\}, \tag{40}$$

$$\begin{aligned}\tilde{M}_{\rm ST}&=\Gamma_fG_0t_{12}G_0t_{34}G_0\Gamma_i\\&\quad+\Gamma_fG_0t_{12}G_0t_{34}G_0t_{12}G_0t_{34}G_0\Gamma_i+\ldots+\{2\leftrightarrow 3\},\end{aligned} \tag{41}$$

where Γ_i and Γ_f are given by (26).

We introduce the notation

$$\begin{aligned}M_{\rm B}&=M_{\rm IPT}+M_{\rm NPT}+M^{\rm B}_{\rm ST}=(\Gamma_f^{24}+\Gamma_f^{34})G_0\Gamma_i\\&=\Gamma_fG_0(\Gamma_i^{12}+\Gamma_i^{31}).\end{aligned} \tag{42}$$

The representation of Eqs. (37)–(41) in the language of 3-dimensional graphs is given in Fig. 7. The amplitude $M^{\rm B}_{\rm ST}$ (40) will henceforth be referred to as the Born amplitude of sequential transfer of a (noninteracting) pair (BST). As shown in the following subsection, the sum of amplitudes $M_{\rm IPT}+M_{\rm NPT}+M^{\rm B}_{\rm ST}$ corresponds to the Born approximation of the standard quantum scattering theory. Along with Eqs. (33) and (34) for the IPT and NPT amplitudes, we give the explicit expression for the BST amplitude in terms of the wave functions:

$$\begin{aligned}M^{\rm B}_{\rm ST}=-(2\pi)^{-3}\int d^3\mathbf{p}_2L_{23}(\mathbf{q}_{23},\mathbf{Q}_1)\{\psi_f^{34^+}\psi_i^{12}\\+\psi_f^{24^+}\psi_i^{13}\}.\end{aligned} \tag{43}$$

In contrast to $M_{\rm B}$, the amplitude $\tilde{M}_{\rm ST}$ contains 4-particle ($NNNN$), 3-particle (NNd), and, in the case of the reaction $p^3{\rm H}\to{}^3{\rm H}p$, 2-particle ($dd$) intermediate states in the S channel. However, we note that, owing to the ordering of the factors t_{ij}, G_0, and t_{kl} in (41) and (42), the individual terms of the amplitude $\tilde{M}_{\rm ST}$ contain only 4- and 3-particle (deuteron pole in the scattering amplitudes t_{ij}) intermediate

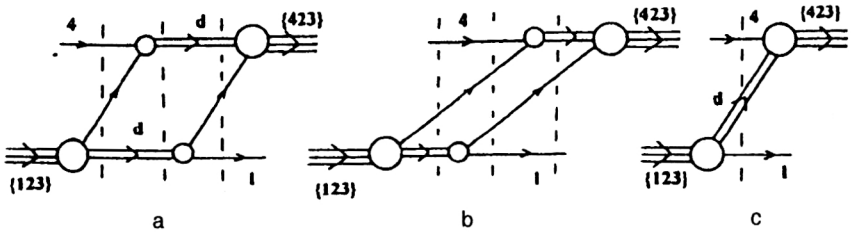

FIG. 8. (a), (b) Intermediate deuteron states in the two-nucleon transfer reaction $p^3\mathrm{H}\to{}^3\mathrm{H}p$; (c) deuteron exchange.

states, and do not contain 2-particle dd states. The intermediate dd state is reproduced only by the entire infinite sum (41) making up part of the amplitude $\tilde{M}_{\mathrm{ST}}$. The contribution of the dd state corresponds to the 3-dimensional graph in Fig. 8a. Meanwhile, the 3-dimensional graph in Fig. 8b, which does not have an intermediate dd state, is contained in the amplitude M_{B}, i.e., in $M_{\mathrm{ST}}^{\mathrm{B}}$.

3.3. Inclusion of the identical nature of the nucleons and the relation to the Born approximation

Let us consider the question of including the Pauli principle in the isospin formalism, assuming that all the nucleons are identical. Equation (27) for the amplitude of NN-pair transfer is asymmetric: it involves the total amplitude for decay of the initial state $R_i=R_i^{12}+R_i^{31}+R_i^{23}$ and the sum of two cut-off fusion amplitudes $R_f^{42}+R_f^{34}$. If we attempt to antisymmetrize the amplitude (27) over the nucleons 1, 2, 3, 4 by hand [by adding the graphs, with the corresponding signs, obtained from (27) by permutation of the particle numbers], we unavoidably obtain the product of the total amplitudes R_i and R_f. Therefore, the result involves the dynamically forbidden combinations $R_f^{23}R_i^{23}$. The inclusion of the Pauli principle in the class of only loop exchange graphs is therefore problematic. The amplitude completely symmetric in the initial and final nucleons can be constructed if to the exchange amplitude (27) we add the amplitude for direct processes, for example, the triangle graph of single pN scattering. Here in the isospin formalism the exchange graph (27) enters into the complete amplitude antisymmetrized in this manner with the combinatorial factor 3 (Ref. 35).

The same result for the combinatorial factor can be obtained by using formal scattering theory in quantum mechanics. In the Born approximation the amplitude for the nucleon-transfer process $4+\{123\}\to 1+\{423\}$ is given by[35]

$$T_{\mathrm{B}}=-3\langle \mathbf{k}'_p\chi(1),\mathbf{k}'_\tau\psi_\tau(4,2,3)|V_{13}+V_{12}|\mathbf{k}_p\chi(4),\mathbf{k}_\tau\psi_\tau(1,2,3)\rangle, \tag{44}$$

where $\mathbf{k}_p$ ($\mathbf{k}'_p$) and $\mathbf{k}_\tau$ ($\mathbf{k}'_\tau$) are the momenta of the initial (final) proton and ^{3}He nucleus, respectively, and χ (χ') are the spin–isospin states of the initial (final) proton. It is easily shown[9] by using the Schrödinger equation for the bound states {123} and {423} that Eq. (44) coincides with the amplitude (42) up to the combinatorial factor of 3:

$$T_{\mathrm{B}}=3M_{\mathrm{B}}, \tag{45}$$

where M_{B} is given by (42). In fact, from the equation for the bound state {123} we have

$$(\hat{V}_{12}+\hat{V}_{13})|\psi_A(1,2,3)\rangle=-(L_{23}(\mathbf{q}_{23},\mathbf{Q}_1)+\hat{V}_{23}|\psi_A(1,2,3)\rangle. \tag{46}$$

Taking into account (46) and also the expression

$$L_{ij}|\psi^{ij}(k;ij)\rangle=-\hat{V}_{ij}|\psi_A(1,2,3)\rangle, \tag{47}$$

we obtain (42) for the matrix element (44) after going to momentum space.

Let us give the more detailed expression for T_{B} which can be obtained from (42) and (45):

$$T_{\mathrm{B}}=6(2\pi)^{-3}\int d^3\mathbf{q}_{23}L_{23}(\mathbf{q}_{23},\mathbf{Q}_1)\chi^+_{p'}(1)\times\{\varphi^{23^+}(4;23)\varphi^{31}(2;31)+\varphi^{42^+}(3;42)\varphi^{31}(2;31)+\varphi^{34^+}(2;34)\varphi^{31}(2;31)\}\chi_p(4). \tag{48}$$

Here the terms $\varphi^{23^+}\varphi^{31}$, $\varphi^{42^+}\varphi^{31}$, and $\varphi^{34^+}\varphi^{31}$ correspond to the IPT, BST, and NPT amplitudes, respectively (see Fig. 7).

3.4. Deuteron exchange

Let us consider the deuteron-exchange graph shown in Fig. 8c. The scattering amplitude t_{23} contains the deuteron pole contribution in the form

$$t_{23}^{\mathrm{pol}}(\mathbf{q},\mathbf{q}',E)=\frac{\varphi_d(\mathbf{q})\varphi_d(\mathbf{q}')(\varepsilon_d+\mathbf{q}^2/2\mu_{23})(\varepsilon_d+\mathbf{q}'^2/2\mu_{23})}{E+\varepsilon_d}, \tag{49}$$

where φ_d and ε_d are the deuteron wave function and binding energy. In order to isolate the contribution of deuteron exchange from the amplitude for interacting-pair transfer, we replace the exact amplitude t_{23} in (21) and (23) for Γ^{23} by the pole term (49), and the same in Eq. (37) for M_{IPT}. As a result, for the desired contribution we find

$$M^{\mathrm{DE}}=-3(\varepsilon-\varepsilon_d+\mathbf{Q}^2_{1;23}/2\mu_{1;23})I^+(\mathbf{Q}_{4;23})I(\mathbf{Q}_{1;23}), \tag{50}$$

where

$$I(\mathbf{Q}_{k;23})=(2\pi)^{-3}\int d^3\mathbf{q}\varphi_d^+(\mathbf{q})\psi^{23}(\mathbf{q},\mathbf{Q}_{k;23}) \tag{51}$$

is the overlap integral of the deuteron wave function $\varphi_d(\mathbf{q})$ with the single Faddeev component ψ^{23} of the {123} bound-state wave function. The combinatorial factor of 3 in (49) takes into account the identical nature of the nucleons in the isospin formalism. This result agrees with that of Ref. 33, according to which the 4-dimensional vertex function of the decay $\{123\}\to\{23\}+1$ into a virtual (off-shell) bound state {23} and a real (on-shell) nucleon is given by the overlap integral (51). The pole amplitude for deuteron exchange

(50)–(51) is contained only in the IPT amplitude $M_{\rm IPT}$ and is not present in the amplitudes $M^{\rm B}_{\rm ST}$ and $M_{\rm NPT}$. However, if in (50) $I(\mathbf{q})$ is replaced by the following overlap integral of the $\{23\}$ bound-state wave function $\varphi_d(\mathbf{q})$ and the full wave function of the nucleus $\{123\}$ ψ_A,

$$I(\mathbf{Q}_{k;23})=(2\pi)^{-3}\int d^{(3)}\mathbf{q}\varphi_D^+(\mathbf{q})\psi_A(\mathbf{q},\mathbf{Q}_{k;23}), \qquad (52)$$

we obtain the usual quantum-mechanical expression for the deuteron-transfer amplitude.[14] This amplitude obviously cannot be obtained from the interacting-pair transfer amplitude $M_{\rm IPT}$, and so it is reproduced by only the sum of all the terms in (27), $M=M_{\rm IPT}+M_{\rm NPT}+M^{\rm B}_{\rm ST}+\tilde{M}_{\rm ST}$, forming a part of it. It is not impossible that the amplitude containing the vertex (52) taken separately might give a better description of the deuteron-transfer mechanism than the amplitude containing the vertex (51) (Ref. 36).

4. THE INCLUSION OF RESCATTERINGS IN THE INITIAL AND FINAL STATES IN THE GLAUBER–SITENKO APPROXIMATION

The dynamics of the np-pair transfer process given by (27) and (39)–(42) does not include rescattering in the initial and final states of this process. We shall use the Schrödinger approach to include these effects. According to the formal theory of potential scattering, the amplitude of the process $p^3{\rm He}\to{}^3{\rm He}p$ taking into account the identical nature of the nucleons can be written as[35]

$$T_{fi}=T^{\rm dir}-3T^{\rm ex}, \qquad (53)$$

where the amplitudes $T^{\rm dir}$ and $T^{\rm ex}$ pertain to processes with nonidentical particles, with $T^{\rm dir}$ describing the direct process $4+\{123\}\to 4+\{123\}$ and $T^{\rm ex}$ describing the "rearrangement" process $4+\{123\}\to 1+\{423\}$. For $T^{\rm ex}$ in post-form we have the expression

$$T^{\rm ex}=\langle f|V_{12}+V_{13}+V_{14}|\varphi_i^{(+)}\rangle, \qquad (54)$$

where $\varphi_i^{(+)}$ is the exact scattering state vector in the system of nonidentical particles $4+\{123\}$, and the vector $|f\rangle$ describes the free state of the system $1+\{423\}$. Applying the Goldberger–Watson theorem[37] to the matrix element (54), we obtain

$$T^{\rm ex}=\langle\chi_f^{(-)}|V_{12}+V_{13}|\varphi_i^{(+)}\rangle+\langle\chi_f^{(-)}|V_{14}|i\rangle, \qquad (55)$$

where $|\chi_f^{(-)}\rangle$ is the state vector of the scattering of nucleon 1 on nucleon 4 bound in the nucleus $\{423\}$, and the vector $|i\rangle$ describes the free motion in the system $4+\{123\}$. The second term in the sum (55) describes exchange processes of the substitution type. The combination $T^{\rm dir}-3\langle\chi_f^{(-)}|V_{14}|i\rangle$ contained in (53) corresponds to the multiple-scattering series with antisymmetrized NN scattering amplitudes. The contribution of these processes has been studied in detail in Ref. 8. In that study satisfactory agreement with the experimental data was obtained for $T_p<1$ GeV, but the contribution of the NN-pair transfer mechanism was neglected. Here we shall restrict ouselves to only the first term in (55). It involves the matrix element describing NN-pair transfer in the process $p\tau\to\tau p$, taking into account the initial- and final-state interactions. The expanded form of this matrix element is

$$T_{fi}^{\rm dist}=-3\langle\tilde{\chi}_f^{(-)}\chi'(1)\psi_A(4,2,3)|V_{12}+V_{13}|\chi(4)\psi_\tau(1,2,3)\tilde{\varphi}_i^{(+)}\rangle. \qquad (56)$$

In the Born approximation, (56) reduces to (44).

Here we include the initial- and final-state interactions in the spirit of Ref. 38. The wave functions $\varphi^{(+)}$ and $\varphi^{(-)}$ are given by the following expressions in momentum space:

$$\tilde{\varphi}_{\mathbf{p}}^{+}(\mathbf{k})=(2\pi)^3\delta^{(3)}(\mathbf{k}-\mathbf{p})+(\mathbf{p}^2-\mathbf{k}^2+i\varepsilon)^{-1}\frac{3}{2}mT_{\mathbf{kp}}^{(+)}, \qquad (57)$$

$$\tilde{\varphi}_{\mathbf{p}'}^{-}(\mathbf{k})=(2\pi)^3\delta^{(3)}(\mathbf{k}-\mathbf{p}')+(\mathbf{p}'^2-\mathbf{k}^2-i\varepsilon)^{-1}mt_{\mathbf{kp}'}^{(-)}. \qquad (58)$$

Here $T_{\mathbf{kp}}$ is the exact t matrix of elastic $N\{3N\}$ scattering, and $t_{\mathbf{kp}}=t_{14}$ is the matrix of off-shell NN scattering on a nucleon bound in the nucleus $\{3N\}$. The main approximations that we use here are the following.

• Since at energies ~ 1 GeV the differential cross section for elastic p^3He scattering is extended in the forward direction and falls off rapidly with increasing scattering angle in the c.m. frame, rescatterings at small angles are most important in the integral (56). Therefore, instead of the exact amplitude $T_{\mathbf{kp}}^{(+)}$ in (56) we use the corresponding approximate expression obtained in the Glauber–Sitenko diffraction theory of multiple scattering.

• The amplitude $t_{\mathbf{kp}}^{(-)}$ is replaced by the on-shell pn scattering amplitude. The pN scattering amplitude in the spinless approximation is parametrized in the form standard for diffraction theory:[39]

$$f_{pN}(q)=\frac{k\sigma_N}{4\pi}(i+\alpha_N)\exp\left(-\frac{1}{2}\beta_N q^2\right), \qquad (59)$$

where q is the momentum transferred in pN scattering, k is the nucleon wave vector in the $p+N$ c.m. frame, σ_N is the total cross section for pN scattering, and α_N and β_N are empirical parameters corresponding to the experimental data on pN scattering.

• As in Ref. 38, after substituting (57) and (58) into (56) we neglect the integrals in the sense of the principal value in k.

With these assumptions the amplitude (56) takes the form

$$\begin{aligned}T_{fi}^{\rm dist}=&T_{\rm B}(\mathbf{p}'_\tau,\mathbf{p}'_p;\mathbf{p}_\tau,\mathbf{p}_p)\\&+\frac{i}{4\pi k_p}\int d^2qF_{p\tau}(\mathbf{q})T_{\rm B}(\mathbf{p}'_\tau,\mathbf{p}'_p;\mathbf{p}_\tau+\mathbf{q},\mathbf{p}_p-\mathbf{q})\\&+\frac{i}{4\pi k_{p'}}\int d^2q'f_{pp}(\mathbf{q}')T_{\rm B}(\mathbf{p}'_\tau-\mathbf{q}',\mathbf{p}'_p\\&+\mathbf{q}';\mathbf{p}_\tau,\mathbf{p}_p)-\frac{1}{(4\pi)^2k_{p'}k_p}\\&\times\int\int d^2qd^2q'F_{p\tau}(\mathbf{q})f_{pp}(\mathbf{q}')T_{\rm B}(\mathbf{p}_\tau-\mathbf{q}',\\&\mathbf{p}'_p+\mathbf{q};\mathbf{p}_\tau+\mathbf{q},\mathbf{p}_p-\mathbf{q}).\end{aligned} \qquad (60)$$

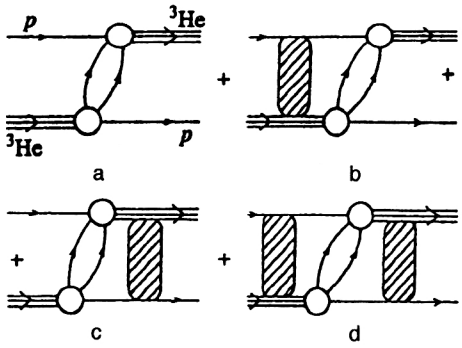

FIG. 9. np-pair transfer in the process $p^3\mathrm{He}\to{}^3\mathrm{He}p$, taking into account rescatterings using (60). (a) Born approximation $M_{\mathrm{IPT}}+M_{\mathrm{NPT}}+M_{\mathrm{ST}}^{\mathrm{B}}$; (b) pN rescattering in the entrance channel; (c) p^3He rescattering in the exit channel; (d) rescattering in the entrance and exit channels.

The last three terms in (60) include rescattering in, respectively, the initial state, the final state, and also the initial and final states simultaneously (see Fig. 9). Using the Gaussian parametrization for the density of the ^{3}He nucleus, the expression for the amplitude $F_{p\tau}$ takes the simple analytic form[40]

$$F_{p\tau}(q)=\sum_{i=1}^{3} A_i e^{-\alpha_i q^2}. \tag{61}$$

Here the parameters A_i and α_i are expressed analytically in terms of the parameters of the NN scattering amplitude (59) and the oscillator radius of the Gaussian form of the ^{3}He density. The three terms in (61) correspond to single, double, and triple collisions of the incident proton with the ^{3}He nucleons.

5. USE OF THE REALISTIC WAVE FUNCTION OF THE ^{3}He NUCLEUS

The completely antisymmetric wave function of a bound state of three nucleons $\{123\}\equiv{}^3$He can be represented as the following sum of Faddeev components:

$$\psi(1,2,3)=\varphi^{23}(1;2,3)+\varphi^{31}(2;3,1)+\varphi^{12}(3;1,2)$$
$$=(1+P_{12}P_{23}+P_{13}P_{32})\varphi^{23}(1;2,3), \tag{62}$$

where

$$\varphi^{ij}(k;i,j)=-\varphi^{ij}(k;j,i)=\varphi^{ij}(\mathbf{q}_{ij},\mathbf{Q}_k), \tag{63}$$

and P_{ij} is the permutation operator for nucleons i and j. We use the following state normalization:

$$\langle\mathbf{p}|\mathbf{p}'\rangle=(2\pi)^3\delta^{(3)}(\mathbf{p}-\mathbf{p}'),\quad \langle\mathbf{r}|\mathbf{p}\rangle=\exp(i\mathbf{pr}),$$
$$\int \psi_A^+(\mathbf{q},\mathbf{Q})\psi_A(\mathbf{q},\mathbf{Q})d\mathbf{q}d\mathbf{Q}=(2\pi)^6, \tag{64}$$
$$\int \varphi_d^+(\mathbf{q})\varphi_d(\mathbf{q})d\mathbf{q}=(2\pi)^3.$$

With this normalization the relation of the amplitudes (48), (54)–(56), and (59) to the differential cross section in the $p+{}^3$He c.m. frame takes the form

TABLE II. Components of the wave function of the ^{3}He nucleus and their quantum numbers.

ν	$(L$	$S)$	I	$(l$	$s)$	j	$(T$	$t)$	$\mathscr{T}$
1	(0	0)	0	(0	$\frac{1}{2}$)	$\frac{1}{2}$	(1	$\frac{1}{2}$)	$\frac{1}{2}$
2	(0	1)	1	(0	$\frac{1}{2}$)	$\frac{1}{2}$	(0	$\frac{1}{2}$)	$\frac{1}{2}$
3	(2	1)	1	(0	$\frac{1}{2}$)	$\frac{1}{2}$	(0	$\frac{1}{2}$)	$\frac{1}{2}$
4	(0	1)	1	(2	$\frac{1}{2}$)	$\frac{1}{2}$	(0	$\frac{1}{2}$)	$\frac{1}{2}$
5	(2	1)	1	(2	$\frac{1}{2}$)	$\frac{1}{2}$	(0	$\frac{1}{2}$)	$\frac{1}{2}$

$$\frac{d\sigma}{d\Omega}=\frac{1}{4\pi^2}\left(\frac{\varepsilon_p\varepsilon_\tau}{\varepsilon_p+\varepsilon_\tau}\right)^2\overline{|T_{fi}|^2}, \tag{65}$$

where $\varepsilon_i=\sqrt{\mathbf{p}_i^2+m_i^2}$ is the total energy of the ith particle in the $p+\tau$ c.m. frame and $\overline{|T_{fi}|^2}$ is the squared modulus of the matrix element averaged over the initial and summed over the final spins.

5.1. The multichannel spin–isospin structure of the np-transfer amplitude

In this section we obtain the expression for the amplitude (48) in the case where the wave function $\psi_A(1,2,3)$ contains several orthogonal terms ν arising in the case of the NN interaction in the $^1S_0$ and $^3S_1-{}^3D_1$ states.

Following Ref. 21, we introduce the following notation for the basis states:

$$ {}_1\langle\mathbf{q}_{23},\mathbf{Q}_1|q_{23},Q_1,\nu\rangle\equiv|[q_{23}(LS)I,Q_1(ls)j]JJ_z;(Tt)\mathscr{T}\mathscr{T}_z\rangle_1$$
$$=\sum_{m_i m_j m_L m_S m_l m_s}(Im_I jm_j|JJ_z)$$
$$\times(Lm_L Sm_S|Im_I)$$
$$\times\left(lm_l\frac{1}{2}m_s\middle|jm_j\right)Y_{Lm_L}(\hat{\mathbf{q}}_{23})$$
$$\times Y_{lm_l}(\hat{\mathbf{Q}}_1)\left|Sm_S,\frac{1}{2}m_s\right\rangle$$
$$\times\left|\left(T\frac{1}{2}\right)\mathscr{T}\mathscr{T}_z\right\rangle_1. \tag{66}$$

Here L, m_L, S, and m_S are the relative orbital angular momentum, the spin, and the corresponding z projections for the pair of nucleons 2 and 3, T is the isospin of this pair; l and m_l are the orbital angular momentum of the spectator nucleon 1 and its z projection; J, J_z, $\mathscr{T}$, and $\mathscr{T}_z$ are the total spin and isospin, and their projections for the nucleus $\{123\}$. The subscript on the state vector $|\rangle_i$ denotes the number of the spectator nucleon, and the index ν denotes the channel number in the jj-coupling scheme

$$\nu\equiv(LS)I(ls)jJJ_z(Tt)\mathscr{T}\mathscr{T}_z \tag{67}$$

and takes the five values $\nu=1,2,\ldots,5$ determined in Ref. 21; these are given in Table II. To calculate the integrals in (48) it is necessary to change to LS coupling. As a result of projection of the first Faddeev component $|\varphi^{23}(1;2,3)\rangle$ of the state (62) on the state $|\mathbf{q}_{23},\mathbf{Q}_1\rangle_1$ we obtain

$$\varphi^{23}(1;2,3)\equiv {}_1\langle \mathbf{q}_{23},\mathbf{Q}_1|\varphi^{23}(1;2,3)\rangle$$

$$=\sum_{\nu_1} {}_1\langle \mathbf{q}_{23},\mathbf{Q}_1|q_{23},Q_1,\nu_1\rangle$$

$$\times\langle q_{23},Q_1,\nu_1|\varphi^{23}(1;2,3)\rangle$$

$$=\sum_{\substack{\nu\mathscr{L}\varphi m_\varphi\\ m_L m_l}} (\mathscr{L}m_{\mathscr{L}}\varphi m_\varphi|JJ_z)(Lm_L lm_l|\mathscr{L}m_{\mathscr{L}})$$

$$\times\begin{pmatrix} L & S & I\\ l & 1/2 & j\\ \mathscr{L} & \varphi & J\end{pmatrix} Y_{Lm_L}(\hat{\mathbf{q}}_{23})Y_{lm_l}(\hat{\mathbf{Q}}_1)$$

$$\times\phi_\nu(q_{23},Q_1)|(s_2s_3)Ss_1,\varphi m_\varphi\rangle_1$$

$$\times|(t_2t_3)Tt,\mathscr{T}\mathscr{T}_z\rangle_1. \qquad (68)$$

In this expression we have transformed to the coupling scheme

$$\mathbf{L}+\mathbf{l}=\mathscr{L},\quad \mathbf{S}+\mathbf{s}_1=\varphi,\quad \mathscr{L}+\varphi=\mathbf{J}, \qquad (69)$$

using the $9j$ symbol and the Clebsch–Gordan coefficients. The spin vector of the state $|(s_2s_3)Ss_1,\varphi m_\varphi\rangle_1$ is an eigenvector of the operators

$$\hat{\mathbf{S}}^2=(\mathbf{s}_2+\mathbf{s}_3)^2,\quad \hat{\mathbf{s}}_1^2,\quad \hat{\varphi}^2,\quad \hat{\varphi}_z. \qquad (70)$$

Similarly, the isospin state $|(t_2t_3)Tt,\mathscr{T}\mathscr{T}_z\rangle_1$ is an eigenvector of the operators

$$\hat{\mathbf{T}}^2=(\mathbf{t}_2+\mathbf{t}_3)^2,\quad \hat{\mathbf{t}}_1^2,\quad \hat{\mathscr{T}}^2=(\hat{\mathbf{T}}+\hat{\mathbf{t}}_1)^2,\quad \hat{\mathscr{T}}_z; \qquad (71)$$

here $\mathbf{s}_i$ and $\mathbf{t}_i$ are the spin and isospin operators of the ith nucleon. The function $\phi_\nu(q_{23},Q_1)$ is the projection of the first Faddeev component $|\varphi^{23}(1;2,3)\rangle$ on the basis state $|q_{23},Q_1;\nu\rangle_1$ in jj coupling. All the other components of the state vectors $|\psi_A(1,2,3)\rangle$ and $|\psi_A(4,2,3)\rangle$ entering into (48) are given by the following scalar products:

$$\varphi^{31}(2;31)={}_1\langle \mathbf{q}_{23},\mathbf{Q}_1|P_{12}P_{23}\varphi^{23}(1;23)\rangle, \qquad (72)$$

$$\varphi^{34}(2;34)={}_4\langle \mathbf{q}_{23},\mathbf{Q}_4|P_{42}P_{23}\varphi^{23}(4;23)\rangle, \qquad (73)$$

$$\varphi^{42}(3;42)={}_4\langle \mathbf{q}_{23},\mathbf{Q}_4|P_{43}P_{32}\varphi^{23}(4;23)\rangle, \qquad (74)$$

$$\varphi^{23}(4;23)={}_4\langle \mathbf{q}_{23},\mathbf{Q}_4|\varphi^{23}(4;23)\rangle. \qquad (75)$$

The result of operation with the permutation operators in (72)–(75) on the spatial variables is calculated by using the expressions

$$P_{12}P_{23}|\mathbf{q}_{23},\mathbf{Q}_1\rangle_1=|\mathbf{q}_{31},\mathbf{Q}_2\rangle_1$$

$$=\left|-\frac{1}{2}\mathbf{q}_{23}+\frac{3}{4}\mathbf{Q}_1,-\mathbf{q}_{23}-\frac{1}{2}\mathbf{Q}_1\right\rangle_1, \qquad (76)$$

$$P_{42}P_{23}|\mathbf{q}_{23},\mathbf{Q}_4\rangle_4=|\mathbf{q}_{34},\mathbf{Q}_2\rangle_4$$

$$=\left|-\frac{1}{2}\mathbf{q}_{23}+\frac{3}{4}\mathbf{Q}_4,-\mathbf{q}_{23}-\frac{1}{2}\mathbf{Q}_4\right\rangle_4, \qquad (77)$$

$$P_{43}P_{32}|\mathbf{q}_{23},\mathbf{Q}_4\rangle_4=|\mathbf{q}_{42},\mathbf{Q}_3\rangle_4$$

$$=\left|-\frac{1}{2}\mathbf{q}_{23}-\frac{3}{4}\mathbf{Q}_4,\mathbf{q}_{23}-\frac{1}{2}\mathbf{Q}_4\right\rangle_4 \qquad (78)$$

The action of the permutation operators on the spin functions is calculated by using the Racah algebra:

$$P_{12}P_{23}|(s_ss_3)Ss_1,\varphi m_\varphi\rangle_1$$

$$=\sum_{s's''}(-1)^{s'+s''}U\left(\frac{1}{2}\frac{1}{2}\varphi\frac{1}{2};s'S\right)$$

$$\times U\left(\frac{1}{2}\frac{1}{2}\varphi\frac{1}{2};s's''\right)|(s_2s_3)s''s_1,\varphi m_\varphi\rangle_1 \qquad (79)$$

$$P_{13}P_{32}|(s_2s_3)Ss_1,\varphi m_\varphi\rangle_1$$

$$=\sum_{s's''}(-1)^{s'+s}U\left(\frac{1}{2}\frac{1}{2}\varphi\frac{1}{2};s'S\right)$$

$$\times U\left(\frac{1}{2}\frac{1}{2}\varphi\frac{1}{2};s's''\right)|(s_2s_3)s''s_1,\varphi m_\varphi\rangle_1, \qquad (80)$$

where $U(j_1j_2jj_3;j_{12}j_{23})$ are the Racah coefficients. The expressions for the isospin functions are similar to these.

Taking into account (66)–(80), the expression for the amplitude (48) takes the form

$$T_{\mathrm{B}}=-6\sum_{\substack{\nu\mathscr{L}\varphi\\ m_Lm_\varphi m_Lm_l}}\sum_{\substack{\nu'\mathscr{L}'\varphi'\\ m'_{\mathscr{L}}m'_\varphi m'_Lm'_l}}\begin{pmatrix} L & S & I\\ l & s & j\\ \mathscr{L} & \varphi & J\end{pmatrix}$$

$$\times\begin{pmatrix} L' & S' & I'\\ l' & s & j'\\ \mathscr{L}' & \varphi' & J'\end{pmatrix}(\mathscr{L}m_{\mathscr{L}}\varphi m_\varphi|JJ_z)$$

$$\times(\mathscr{L}'m'_{\mathscr{L}}\varphi'm'_\varphi|JJ'_z)(Lm_Llm_l|\mathscr{L}m_{\mathscr{L}})$$

$$\times(L'm'_Ll'm'_l|\mathscr{L}'m'_{\mathscr{L}})\{B_SB_TI^{4;23}_{2;31}(Q_4,Q_1)$$

$$+A_SA_TI^{3;42}_{2;31}(Q_4,Q_1)+\tilde{A}_S\tilde{A}_TI^{2;34}_{2;31}(Q_4,Q_1)\}. \qquad (81)$$

Here we have used the notation

$$B_S\equiv B_S(s'\varphi'm'_\varphi\sigma';s\varphi m_\varphi\sigma)$$

$$=\sum_{\bar{s}'m'_s}U\left(\frac{1}{2}\frac{1}{2}\varphi\frac{1}{2};\bar{s}'s\right)U\left(\frac{1}{2}\frac{1}{2}\varphi\frac{1}{2};\bar{s}'s'\right)$$

$$\times\left(s'm'_s\frac{1}{2}\sigma\middle|\varphi'm'_\varphi\right)\left(s'm'_s\frac{1}{2}\sigma'\middle|\varphi m_\varphi\right); \qquad (82)$$

$$A_S\equiv A_S(s'\varphi'm'_\varphi\sigma';s\varphi m_\varphi\sigma)$$

$$=\sum_{\bar{s}'\bar{s}''\bar{s}'\bar{m}''_s}U\left(\frac{1}{2}\frac{1}{2}\varphi\frac{1}{2};\bar{s}'\right)U\left(\frac{1}{2}\frac{1}{2}\varphi\frac{1}{2};\bar{s}'\bar{s}''\right)$$

$$\times U\left(\frac{1}{2}\frac{1}{2}\varphi\frac{1}{2};\tilde{s}'s'\right)U\left(\frac{1}{2}\frac{1}{2}\varphi\frac{1}{2};\tilde{s}'\bar{s}''\right)$$

$$\times\left(\bar{s}''\bar{m}''_s\frac{1}{2}\sigma\middle|\varphi'm'_\varphi\right)\left(\bar{s}''\bar{m}''_s\frac{1}{2}\sigma'\middle|\varphi m_\varphi\right)$$

TABLE III. Expansion coefficients of the functions (86).

ν	ϕ_ν		χ_ν	
	A_i, $F^{L+3/2}$	α_i, F^2	A_i, $F^{L+3/2}$	α_i, F^2
1	2.413615	5.535106	4.20690	7.62335
	−1.299993 E−01	1.060713 E−01	2.59354	2.37678
	4.118231 E−02	4.555083 E−03	4.8189 E−01	9.18116 E−01
	1.762614 E−00	1.611916 E+00	−2.45993 E−02	1.60613 E−01
	7.491376 E−01	5.466668 E−01	5.21600 E−03	1.40849 E−02
	−4.00000 E−02	4.526665 E−03	−5.67292 E−03	1.03918 E−02
	−3.451822 E−02	5.023824 E−02	2.17920 E−03	7.19787 E−03
2	−2.54039	6.55162	6.51121	9.38385
	−1.93783	1.74914	2.59354	3.04139
	−7.74249 E−01	5.72939 E−01	5.45100 E−01	1.22803
	1.12706 E−01	1.15040 E−01	−2.40357 E−02	1.85314 E−01
	3.09857 E−02	5.11790 E−02	1.56646 E−03	1.84247 E−02
	−6.4000 E−03	3.94752 E−02	−2.61864 E−03	1.03918 E−02
	1.18765 E−03	6.58383 E−03	2.17920 E−03	9.12018 E−03
3	2.28664	5.24865	4.72099 E+00	8.07017 E+00
	1.58851	1.54274	2.26885 E+00	2.16948 E+00
	4.01584 E−01	5.17267 E−01	5.47433 E−01	8.19032 E−01
	3.9092 E−02	1.83278 E−01	−6.83070 E−02	1.22875 E−02
	2.05881 E−02	2.06735 E−01	−4.40191 E−02	1.52207 E−01
	8.00270 E−05	3.0200 E−02	6.95022 E−02	1.26212 E−02
			2.18650 E−03	7.21084 E−03
			−2.72200E−05	1.01611 E−02
4	−8.70495 E−01	3.71583	15.9474 E+00	10.3187 E+00
	−1.25478 E+00	1.26227	7.84362 E+00	2.97959 E+00
	−1.06957 E+00	4.80049 E−01	1.14908 E+00	1.00653
	2.61178 E−01	1.17920 E−01	1.08556 E−01	3.67967−01
	8.00414 E−02	5.79416 E−02	8.77166 E−03	1.47078 E−01
	−3.15296 E−03	5.18526 E−03	5.44178 E−04	6.09059 E−02
	4.00142 E−04	6.4000 E−04	1.83200 E−05	2.19665 E−02
5	2.60888 E−01	5.88278	6.11461 E+00	9.63587 E+00
	6.37050 E−01	1.30323	4.11932 E+00	3.01398 E+00
	2.34628 E−01	4.35207 E−01	1.45378 E+00	1.16701 E+00
	4.83235 E−02	1.58004 E−01	3.20978 E−01	5.33558 E−01
	6.72.416 E−02	3.64735 E−01	4.16811 E−02	2.60074 E−01
			−8.11338 E−04	5.45882 E−02
			−6.70900 E−05	1.99625 E−02

$$\times(-1)^{s'}(-1)^{\bar{s}'+\bar{s}'+\bar{s}''}. \tag{83}$$

The expression for $\tilde{A}_S$ differs from (83) by the replacement $(-1)^{s'}\to(-1)^{\bar{s}''}$ inside the summation. The isospin factors B_T, A_T, and $\tilde{A}_T$ as functions of T', $\mathscr{T}'$, $\mathscr{T}'_z$, τ', and T are defined analogously. The spatial integrals in (81) have the form

$$I^{k';i'j'}_{k;ij}=(2\pi)^{-3}\int d\mathbf{q}_{23}Y^*_{L'M'}(\hat{\mathbf{q}}_{i'j'})Y^*_{l'm'}(\hat{\mathbf{Q}}_{l'm'})$$
$$\times\Phi_{\nu'}(|\mathbf{q}_{i'j'}|,|\mathbf{Q}_{k'}|)Y_{LM}(\hat{\mathbf{q}}_{ij})Y_{lm}(\hat{\mathbf{Q}}_k)\Phi_\nu(|\mathbf{q}_{ij}|,|\mathbf{Q}_k)$$
$$\times L_{23}(\mathbf{q}_{23},\mathbf{Q}_1). \tag{84}$$

Here the sets of variables $(\mathbf{q}_{42},\mathbf{Q}_3)$, $(\mathbf{q}_{34},\mathbf{Q}_2)$, and $(\mathbf{q}_{31},\mathbf{Q}_2)$ are linear combinations of the momenta $\mathbf{q}_{23}$, $\mathbf{Q}_4$, and $\mathbf{Q}_1$ according to (76)–(78). The integral (84) is calculated using the following separable parametrization of the wave function $\Phi_\nu(q,Q)$:

$$\Phi_\nu(q,Q)=n_\nu\phi_\nu(q)\chi_\nu(Q), \tag{85}$$

constructed in Ref. 41, where the functions ϕ and χ were approximated as sums of pole terms. We have used the results of Ref. 41 to construct the Gaussian parametrization of the functions $\{\phi_\nu(p),\chi_\nu(p)\}=f_\nu(p)$:

$$f_\nu(p)=\sum_i A_i\exp(-\alpha_i p^2), \quad S \text{ wave}$$
$$f_\nu(p)=p^2\sum_i A_i\exp(-\alpha_i p^2), \quad D \text{ wave}. \tag{86}$$

The expansion coefficients in (86) are given in Table III. These coefficients are found by minimizing the difference of the convolutions

$$I(\mathbf{Q})=\int f_\nu(\mathbf{q})f_\nu(\mathbf{q}+\mathbf{Q})d\mathbf{q}, \tag{87}$$

calculated in the range $Q=0-13\ \mathrm{F}^{-1}$, using, on the one hand, the functions $f_\nu(p)=\{\phi_\nu(p),\chi_\nu(p)\}$ from Ref. 41 and, on the other, the parametrization (86).

When only the IPT contribution is included [this corresponds to the first term in (81)] in the S-wave approximation for the wave function, Eq. (81) reduces exactly to Eq. (7) of Ref. 42.

5.2. The inclusion of relativistic effects

Equations (48) and (56) depend on the momenta $\mathbf{Q}_1$ and $\mathbf{Q}_4$, which are the momenta of nucleons 1 and 4 in the $\{1+2+3\}$ and $\{4+2+3\}$ c.m. frames, respectively. In the nonrelativistic approach these momenta are given by

$$\mathbf{Q}_1=\tfrac{1}{3}\,\mathbf{p}_\tau-\mathbf{p}'_p,\quad \mathbf{Q}_4=\tfrac{1}{3}\,\mathbf{p}_{\tau'}-\mathbf{p}_p, \tag{88}$$

where $\mathbf{p}_p$ ($\mathbf{p}'_p$) and $\mathbf{p}_\tau$ ($\mathbf{p}'_\tau$) are the initial (final) momenta of the proton and ^{3}He nucleus in the $p+{}^3$He c.m. frame.

At large momentum transfers ($\Delta\geqslant m$) relativistic effects can play a significant role in the dynamics of the process. These effects can be included most systematically by using the relativistic quantum mechanics of systems with a fixed number of particles.[24,43] One example of the use of this approach is the description of backward elastic pd scattering within the framework of neutron exchange.[4,44] The results of Ref. 43 make it possible in principle to calculate the ^{3}He (^{3}H) wave function by solving relativistic equations of the Faddeev type. With this function it is then possible to construct a systematic relativistic generalization of the np-exchange mechanism in backward p^3He scattering by using four-body relativistic quantum mechanics. However, technically this problem is very complicated. Here we shall limit ourselves to only an estimate of the contribution of relativistic effects. For this, after integrating over $\mathbf{q}_{23}$ in (48) and (56), in the final result we replace the nonrelativistic expressions (88) for the momenta $\mathbf{Q}_1$ and $\mathbf{Q}_4$ by the corresponding relativistic expressions (8): $\mathbf{Q}_1=\mathbf{q}$, $\mathbf{Q}_4=\mathbf{q}'$. We note that the moduli of the momenta (8) are always numerically smaller (for $\theta_{\mathrm{c.m.}}=180°$) than the corresponding nonrelativistic values.

6. THE RESULTS OF NUMERICAL CALCULATIONS AND DISCUSSION

6.1. Low energies

Backward elastic p^3He and p^3H scattering at energies $\sim$10 MeV was studied theoretically earlier in Refs. 42 and 45 from the viewpoint of the traditional problems arising in few-body systems with strong interactions. The question of whether or not such processes can be described without resorting to the exact solution of the Faddeev–Yakubovskiĭ equations, but by including only a few fairly simple Feynman graphs, was studied. This turned out to be possible within the multichannel K-matrix approach.[46] The procedure essentially reduces to the inclusion of a limited number of channels, the amplitudes for transitions between which satisfy a system of coupled Heitler equations. This system ensures unitarity of the S matrix for any number of included channels. One of the main dynamical assumptions in this approach is that the K-matrix element in a particular channel can be identified with the simplest Feynman graph (the Born approximation) for the T matrix in that channel. Actual calculations showed that this approach is suitable for describing a number of low-energy processes: $d(d,p)^3$H, ^{3}He$(p,p)^3$He, ^{3}H$(p,n)^3$He, and ^{4}He$(p,p)^4$He. It should be noted that a quantitative description of the differential cross section of elastic p^3He and n^3H scattering in the angular range $\theta_{\mathrm{c.m.}}=0-180°$ has also been obtained by the resonating-group method in Ref. 47. However, so-called effective forces without tensor forces were used instead of realistic ones. As shown in Ref. 48, in the description of resonances in $n\alpha$ scattering, the inclusion of tensor forces significantly changes the predictions from those of the case when effective forces are used.

Backward elastic p^3He scattering was studied in Refs. 42 and 45 using the K-matrix approach in the one-channel approximation. Here an element of the K matrix was taken to be the element of the T matrix describing the transfer of an interacting pair, $T_{\mathrm{IPT}}=3M_{\mathrm{IPT}}$. The exchange of a noninteracting pair was included in Ref. 28. Since Eq. (48) for T_{B} is real, according to the rules of the K-matrix approach it can be used as the element of the K matrix in the elastic channel. The transition to the inelastic two-particle $d+d$ channel is isospin-forbidden, and, following Refs. 42 and 45, we shall not consider the coupling to the 3-particle $(2N+d)$ and 4-particle $(4N)$ channels opened at energies $T_p=8.5$ and 11.5 MeV. Finally, in the one-channel approximation, after expanding the elements of the unitarized T matrix in partial waves, we obtain (dropping the spin–isospin factors)

$$T^l_{fi}=\frac{K_l}{1+3imQ_{p\tau}K_l/8\pi}, \tag{89}$$

where m is the nucleon mass, $Q_{p\tau}$ is the relative momentum in the $p+{}^3$He channel, and

$$K_l=\frac{1}{2}\int_{-1}^{1}T_{\mathrm{B}}(z)P_l(z)dz. \tag{90}$$

The maximum number of partial waves in the calculations of Ref. 28 is $l_{\max}=8$.

The results of the calculations are shown in Figs. 10 and 11. We arrive at the following conclusions. Even at very low energies ($\sim$2 MeV) the contribution of noninteracting-pair exchange is comparable to the IPT contributions. As the energy increases the relative contribution of noninteracting-pair transfer grows and becomes dominant at $T_p\sim30$ MeV. The calculated IPT contribution to the cross section is about 1.5–2 times smaller than in Ref. 42 at $T_p=10-30$ MeV and its absolute value does not reach the experimental points at any of the energies studied. Since the IPT expressions are identical to the expressions of Ref. 42, this result is entirely due to the difference of the ^{3}He wave functions used in Refs. 42 and 28. Here two important things should be noted. First, the "machine" wave functions used in Ref. 42 have the correct 3-particle asymptote, in contrast to the parametrization of Ref. 41. However, this is apparently important only for imaginary values of the momenta q_{ij} and Q_k, for example, in calculating the on-shell vertex function for tritium decay into three nucleons, $^3\mathrm{H}\to n+p+n$ (Ref. 50). At small

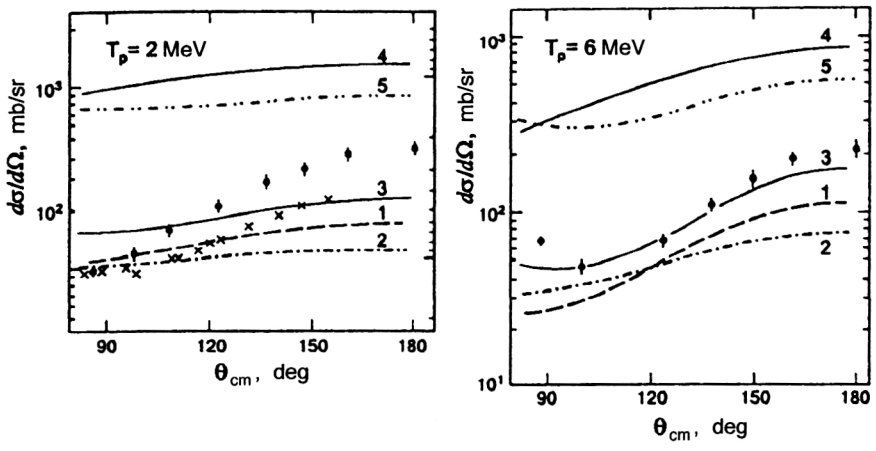

FIG. 10. Experimental data on elastic n^3He scattering (×) and p^3He scattering (●) at $T_p = 2$ and 6 MeV from Ref. 49, compared with the results of calculations using unitarized amplitudes: (*1*) the IPT contribution; (*2*) BST+NPT; (*3*) IPT+BST+NPT. Curves *4* and *5* were obtained in the Born approximation: (*4*) IPT+BST+NPT; (*5*) single scattering+IPT +BST+NPT.

real values of q_{ij} and Q_k the parametrization of Ref. 41 and the initial wave function of Ref. 21 give identical results, as seen, for example, from calculations of the ^{3}He elastic form factor.[41] Meanwhile, the pole singularities of the pair T matrix in the singlet and triplet channels, which are very important for the IPT contribution, are reproduced correctly by the parametrization of Ref. 41, which follows directly from the table of coefficients for this function (see Ref. 41). The second source of discrepancy might be related to the fact that in Ref. 42 potentials without tensor forces were used in the triplet $^3S_1$ channel of the NN interaction. This is very important, because this discrepancy increases with increasing initial energy.

After unitarization, the coherent sum of the IPT contributions and noninteracting-pair exchange reproduces the shape of the differential cross section in the backward hemisphere $\theta_{\text{c.m.}} \geqslant 120°$, and at low energies ($T_p \sim 6-10$ MeV) also satisfactorily describes its absolute value. As can be seen from Fig. 11, at 19.5 MeV unitarized pn-pair exchange gives a differential cross section with magnitude ~ 2 times greater than experiment. For $T_p = 30.6$ MeV the discrepancy becomes even greater. This might be related to enhancement of the role of 3- and 4-particle channels in this energy range, the contribution of which to the K-matrix calculations was neglected. Finally, the contribution of single pN scattering calculated in Ref. 28 at energies of 2 and 6 MeV, taking into account the $^1S_0$ and $^3S_1$ phase shifts in NN scattering, is also comparable in magnitude to the contribution of pn-pair transfer. As shown in Ref. 28, the inclusion of this contribution in the Born approximation eliminates the disagreement between theory and experiment.

6.2. Intermediate energies

Numerical calculations were performed using the 5-channel ^{3}He wave function obtained in Ref. 21 by solving the Faddeev equations in momentum space. The results of the calculations of the differential cross section for p^3He scattering at $\theta_{\text{c.m.}} = 180°$ as a function of the initial proton energy in the lab frame T_p, obtained by neglecting rescattering in the initial and final states, are shown in Figs. 12–14.

The contribution of the DE mechanism with the overlap integrals (51) and (52) is shown in Fig. 12. The results of the calculations using the IPT, NPT, and BST mechanisms in the S-wave approximation are compared with the experimental data in Fig. 13. The role of the D component of the ^{3}He wave function is shown in the same figure for the case of the IPT and BST mechanisms. All the theoretical curves in Figs. 12, 13, 15, and 16 were obtained using relativistic momenta (8). The results of the calculations using nonrelativistic momenta (88) for the case of the IPT and BST mechanisms are

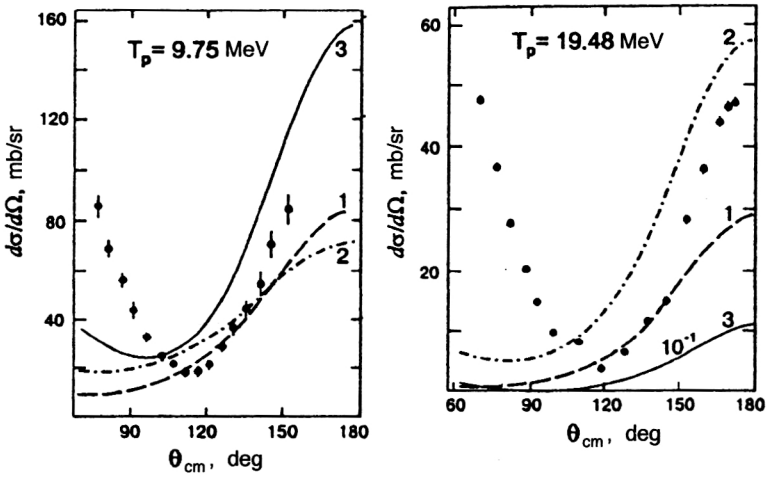

FIG. 11. The same as in Fig. 10, but at the energies $T_p = 9.75$ and 19.48 MeV. The points (●) are the experimental data from Ref. 42.

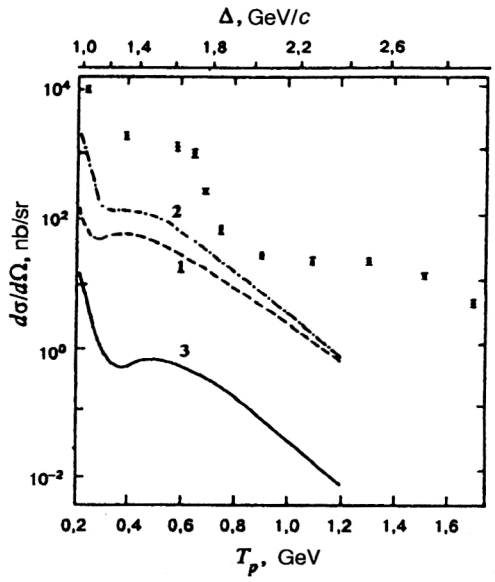

FIG. 12. Differential cross section for elastic p^3He scattering in the c.m. frame at angle $\theta_{c.m.} = 180°$ as a function of the initial proton kinetic energy T_p and the momentum transfer Δ. The curves show the results of the calculations neglecting rescattering: (1) IPT ($S+D$) with the S and D components of the ^{3}He wave function; (2) DE ($S+D$) with the overlap integral (52); (3) DE ($S+D$) with the overlap integral (51). The points are the experimental data from Ref. 1.

compared with the analogous calculations with relativistic momenta (8) in Fig. 14.

Figures 12–14 lead to the following conclusions.

First, we see from Fig. 12 that for the overlap integral (52) the cross section calculated using the DE mechanism is about two orders of magnitude larger than that calculated using the integral (51) and is comparable to that calculated for the IPT mechanism. However, the DE contribution is significantly smaller in absolute value than the experimental

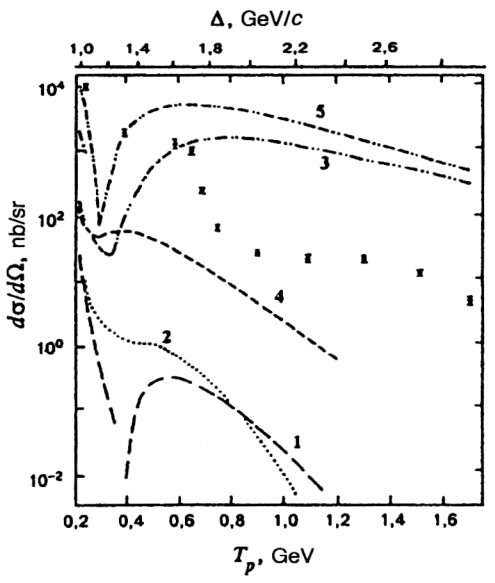

FIG. 13. The same as in Fig. 12, except that the curves are the following: (1) IPT (S) with the S component of the ^{3}He wave function; (2) NPT (S); (3) BST (S); (4) IPT ($S+D$); (5) BST ($S+D$).

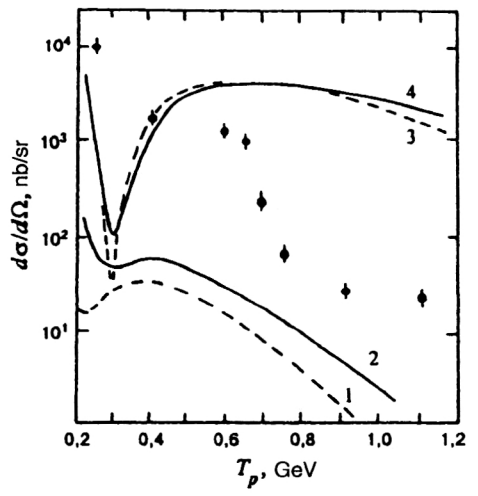

FIG. 14. The same as in Fig. 12, except that the curves are the following: (1), (2) IPT ($S+D$); (3), (4) BST+NPT with the $S+D$ components of the ^{3}He wave function. The dashed lines 1 and 3 were obtained using the nonrelativistic momenta (88), and the solid lines 2 and 4 were obtained using the relativistic momenta (8).

data in the entire energy range studied, and the form of its energy dependence does not agree with experiment.

Second, when the initial- and final-state interactions are neglected, the BST mechanism dominates. Its contribution in the energy range 0.7–1.7 GeV falls off quite slowly with increasing initial energy and in the Born approximation is almost two orders of magnitude higher than the experimental points.[1] On the other hand, the contributions of the IPT and NPT mechanisms and also of deuteron exchange (DE) decrease rapidly with increasing energy. They lie below the experimental points, and their energy dependence differs significantly from the experimental one.

Third, the BST contribution is insensitive to inclusion of the D component of the ^{3}He wave function. Curve *3* in Fig. 13, which shows the BST contribution taking into account only the S components of the ^{3}He wave function, does not differ qualitatively from curve 5 obtained for the BST

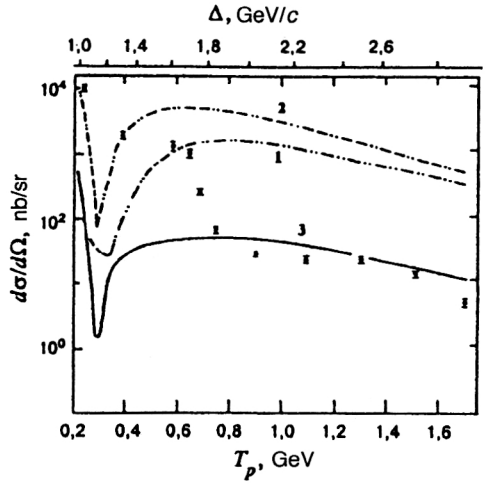

FIG. 15. The same as in Figs. 12–14, except that the curves are the following: (1) IPT+NPT+BST with S components; (2) IPT+NPT+BST with $S+D$ components; (3) IPT+NPT+BST (S) including Glauber rescattering.

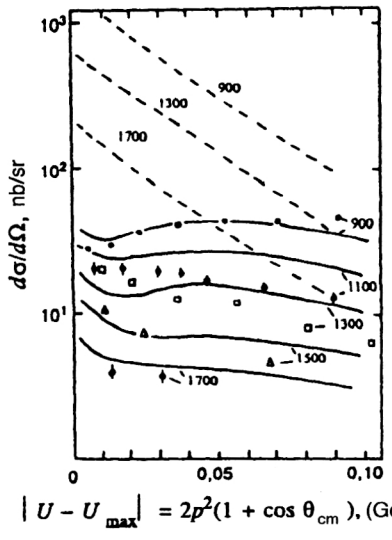

FIG. 16. Differential cross section for elastic p^3He scattering in the backward hemisphere at various initial energies, whose values in MeV are given near the curves. The curves were calculated using the sum of mechanisms IPT+NPT+BST in the S-wave approximation for the ^{3}He wave function. The dashed lines are the Born approximation, and the solid lines include Glauber rescattering; p is the proton momentum in the c.m. frame, and $\theta_{c.m.}$ is the scattering angle. The experimental points are taken from Ref. 1.

mechanism including the S and D components of the wave function. Meanwhile, curve 5 is practically the same as the result predicted by the sum of all three mechanisms IPT+NPT+BST taking into account the S and D components (curve *2* in Fig. 15). Comparison of curves *1* and *4* in Fig. 13 shows that the contribution of the IPT mechanism to the reaction cross section is increased by about two orders of magnitude when the D component of the ^{3}He wave function is switched on. The role played by the D component is similar also for the NPT and DE mechanisms.

Fourth, when relativistic effects are included, the BST contribution is increased by no more than 20–30%, while the contribution of the other mechanisms is increased by 3–5 times. The result remains lower than the experimental data.

The formal reason for this special behavior of the BST mechanism compared to the other mechanisms is the following. The term $\varphi_f^{42^+}\varphi_i^{31}$ inside the integral in (48) corresponding to the BST contribution has arguments with the following structure:

$$\varphi_f^{42^+}\varphi_i^{31}=\varphi_f^{42^+}\left(-\frac{1}{2}\mathbf{q}_{23}-\frac{3}{4}\mathbf{Q}_4,\mathbf{q}_{23}-\frac{1}{2}\mathbf{Q}_4\right)\times\varphi_i^{31}\left(-\frac{1}{2}\mathbf{q}_{23}+\frac{3}{4}\mathbf{Q}_1,-\mathbf{q}_{23}-\frac{1}{2}\mathbf{Q}_1\right). \quad (91)$$

The other two terms corresponding to the NPT and IPT mechanisms have the form

$$\varphi_f^{34^+}\varphi_i^{31}=\varphi_f^{34^+}\left(-\frac{1}{2}\mathbf{q}_{23}+\frac{3}{4}\mathbf{Q}_4,-\mathbf{q}_{23}-\frac{1}{2}\mathbf{Q}_4\right)\times\varphi_i^{31}\left(-\frac{1}{2}\mathbf{q}_{23}+\frac{3}{4}\mathbf{Q}_1,-\mathbf{q}_{23}-\frac{1}{2}\mathbf{Q}_1\right), \quad (92)$$

and

$$\varphi_f^{23^+}\varphi_i^{31}=\varphi_f^{23^+}(\mathbf{q}_{23},\mathbf{Q}_4)\varphi_i^{31}\left(-\frac{1}{2}\mathbf{q}_{23}+\frac{3}{4}\mathbf{Q}_1,-\mathbf{q}_{23}-\frac{1}{2}\mathbf{Q}_1\right). \quad (93)$$

For scattering at $\theta_{c.m.}=180°$, from (88) we find $\mathbf{Q}_4=-\mathbf{Q}_1$. With this condition Eq. (91) differs from (92) and (93) in that in the integration over $\mathbf{q}_{23}$ any two of the four momenta can simultaneously vanish (for example, at the point $\mathbf{q}_{23}=\frac{3}{2}\mathbf{Q}_1$ we have $-\frac{1}{2}\mathbf{q}_{23}-\frac{3}{4}\mathbf{Q}_4=0$ and $-\frac{1}{2}\mathbf{q}_{23}+\frac{3}{4}\mathbf{Q}_1=0$). In Eqs. (92) and (93) only one of the momenta can vanish, while the other three take values $\sim|\mathbf{Q}_1|=|\mathbf{Q}_4|$. In the kinematical range studied, $T_p=0.7-1.7$ GeV, the momenta $|\mathbf{Q}_1|$ and $|\mathbf{Q}_4|$ have rather large values ~ 0.5 GeV/c. The wave function $\varphi^{ij}(\mathbf{q},\mathbf{Q})$ falls off rapidly with increasing $|\mathbf{q}|$ or $|\mathbf{Q}|$. From this we conclude that the contribution of the term (91) to the integral (48) does actually dominate.

Obviously, in the region $\theta_{c.m.}<180°$, in which the equation $\mathbf{Q}_1=-\mathbf{Q}_4$ is violated, the BST mechanism does not have this preeminence. The angular dependence of backward elastic p^3He scattering as a function of the variable $u=p^2(1+\cos\theta^2)$ is shown in Fig. 16. We see that the contribution of the BST mechanism in the Born approximation (dashed lines) does actually fall off rapidly with increasing scattering angle.

At first sight, the features of the BST mechanism listed above indicate that for scattering at angle $\theta_{c.m.}=180°$ this mechanism does not require high-momentum components of the ^{3}He wave function even at the large momentum transfer $\Delta=2-3$ GeV/c which occurs in the studied process at energies $T_p=1.0-1.7$ GeV. However, as was shown recently by the present author,[51] this is only partially correct. For $T_p>1$ GeV the amplitude of the BST mechanism is determined mainly by the values of the Faddeev component of the wave function $\varphi^{23}(\mathbf{q}_{23},\mathbf{Q}_1)$ at large relative momenta $q_{23}>0.6$ GeV/c of the NN pair in the $^1S_0$ state and at small "spectator" momenta $Q_1\sim 0-0.2$ GeV/c.

The numerical calculations taking into account Glauber–Sitenko rescatterings in the initial and final states are compared with the Born approximation and the experimental data in Figs. 15 and 16. Here the amplitude of elastic p^3He scattering at small angles includes only the S components of the ^{3}He wave function. The numerical results were obtained using the parameters of the NN amplitudes (59) from Ref. 52 in the energy range $T_p=0.3-1$ GeV and from Ref. 53 in the range $T_p\geq 0.4$ GeV with Gaussian density for the ^{3}He nucleus from Ref. 54. Direct calculations show that the use of these parameters leads to a good description of the data on forward elastic p^3He scattering at energies 0.4–1.0 GeV in the vicinity of the first two diffraction peaks ($\theta_{c.m.}=0-60°$; Refs. 8 and 54).

As seen from Fig. 15, when Glauber rescatterings are included the differential cross section for the angle $\theta_{c.m.}=180°$ given by the sum IPT+NPT+BST does not change its shape, but its absolute value is decreased by 30–50 times. Roughly the same suppression of the absolute value of the cross section due to the inclusion of the initial- and final-state interactions in the eikonal approximation was observed in elastic $p\alpha$ scattering for the tritium exchange mechanism.[22] As a result, in the range $T_p=0.9-1.7$ GeV the

theoretical curve agrees qualitatively with the experimental data in absolute value. As can be seen from Fig. 16, when rescattering is included, the angular dependence becomes smoother and also agrees qualitatively with the experimental data for angles $\theta_{\text{c.m.}} \approx 160-180°$. The reason for the smoothing out of the cross section as the scattering angle $\theta_{\text{c.m.}}$ deviates from 180° is discussed in detail in Ref. 12 for the example of backward elastic pd scattering. At energies $T_p \leqslant 0.9$ GeV the contribution of the np-pair transfer mechanism to the cross section at $\theta_{\text{c.m.}} = 180°$ is greatly suppressed, owing to the deep minimum at ~ 0.3 GeV. In this energy range ($T_p \leqslant 0.9$ GeV) the multiple pN-scattering mechanism taking into account the antisymmetrization of the pN amplitudes, discussed in Refs. 8 and 54, apparently gives the dominant contribution to backward elastic p^3He scattering.

6.3. The appearance of $\hat{A}\{d^*+p\}$ structure of the ^{3}He nucleus in backward p^3He scattering

The sensitivity of the pn-transfer mechanism to the form of the ^{3}He wave function was studied in Ref. 31. Here, in addition to the Faddeev wave function,[21] cluster models of the form $\Psi_1 = \hat{A}\{d+p\}$ and $\Psi_2 = \hat{A}\{d^*+p\}$ and superpositions of them were used.

If in the second part of (62) the Faddeev component $\varphi^{23}(\mathbf{q}_{23}, \mathbf{Q}_1)$ is replaced by some vectorially coupled (in the jj scheme) product of the wave function of the real deuteron $\varphi_d(2,3)$, the function describing the relative motion of the deuteron and nucleon 1, $f(\mathbf{Q}_1)$, and the spin–isospin function of nucleon 1, $\chi_p(1)$, then for the ^{3}He nucleus we obtain the wave function of the cluster model:

$$\Psi_1 = \hat{A}\{\varphi_d(\mathbf{q}_{23} f(\mathbf{Q}_1)\chi_p(1)\}. \tag{94}$$

Here for brevity we have omitted the angular momenta and the Clebsch–Gordan coefficients. Such functions are widely used to calculate the structure of light nuclei by the resonating-group method (RGM).[55] The function (94) is completely antisymmetrized and has the structure (62). However, in contrast to the Faddeev wave function,[21] the cluster wave function (94) includes only 4 channels—the first channel according to the classification of Ref. 21 and corresponding to the state of the pair of nucleons 2 and 3 with quantum numbers $L=S=0$, $T=1$, is absent.[1)] The inclusion of this state corresponds to the RGM calculation with channel coupling:[55]

$$\Psi_2 = \hat{A}\{\varphi_d(\mathbf{q}_{23} f(\mathbf{Q}_1)\chi_p(1)\} + \delta\hat{A}\{\varphi_{d*}(\mathbf{q}_{23})\tilde{f}(\mathbf{Q}_1)\chi_p(1)\}. \tag{95}$$

Here the wave function φ_{d*} describes the internal motion of the nucleon pair {23} in the $^1S_0$ state. The relative motion of the center of mass of this pair and the first nucleon is described by the function $\tilde{f}$.

It should be emphasized that the amplitude $M^{\text{B}}_{\text{ST}} + \tilde{M}_{\text{ST}}$ exactly reduces to zero if the $\nu = 1$ channel corresponding to the configuration $\{NN(^1S_0)+N\}$ is excluded from the ^{3}He wave function. This follows from the isotopic structure of the ST graphs in Fig. 7, in particular, from the fact that the lower or upper NN loops of these graphs in the process $p^3\text{He} \to {}^3\text{He}p$ are two-proton loops, i.e., they correspond to a state with isospin $T=1$. On the other hand, the NPT graph (like the IPT graph) is not essential to the weight of the configuration $\{NN(^1S_0)+N\}$, because for these mechanisms both NN loops can simultaneously be in pn states with isospin $T=0$.

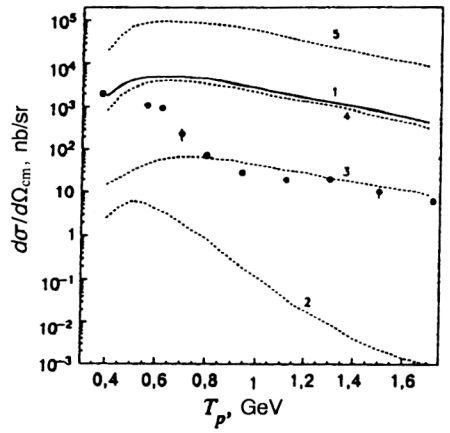

FIG. 17. Differential cross section for backward elastic p^3He scattering at the angle $\theta_{\text{c.m.}} = 180°$ as a function of the initial proton energy T_p. The results of the calculations using Faddeev (curve 1) and cluster (curves 2–5) wave functions are for the summed contribution of the mechanisms IPT+NPT+BST. (2) $\delta=0$; (3) $\delta=0.17$; (4) $\delta=0.5$; (5) $\delta=1$. The points are the experimental data of Ref. 1.

In Ref. 31 the following approximations were used for the cluster functions (94) and (95). The deuteron wave function φ_d in the Reid soft-core potential with S and D components was taken from Ref. 57. The relative-motion function $f(\mathbf{Q})$ was determined by the overlap integral of the deuteron and ^{3}He wave functions (1).

The wave functions φ_{d*} and $\tilde{f}$ in (95) and the numerical value of δ must be determined from the three-particle dynamics. However, for a qualitative estimate, and also to check how sensitive the amplitude (48) is to the form of the wave function, in the cluster model we take $\varphi^*_d = \varphi_s$ and $\tilde{f} = f_0$, where φ_s and f_0 are the S components of the deuteron wave function and the overlap integral (1), respectively. The quantity δ is treated as a free parameter for unit norm of the function (1).

The results of the calculations, presented in Fig. 17, show that the contribution of the BST mechanism is very sensitive to the value of δ. For $\delta=0$ the differential cross section contains only the contributions of the IPT and NPT mechanisms and lies considerably lower than the experimental data. As δ increases the contribution of the pn-transfer mechanism grows rapidly, exclusively owing to the BST amplitude. It should be stressed that for $\delta=0.5$ the results of the calculations using the three-body Faddeev function[41] and the model function (95) are practically indistinguishable. Remarkably, it is at this value of δ that the relative weight of the first ($L=S=0$, $T=1$) and second ($L=0$, $S=1$, $T=0$) channels in the normalization of the wave function (95) are the same as in the Faddeev wave function. It can therefore be

concluded that the cross section for p^3He scattering at $\theta_{c.m.} = 180°$ for $T_p = 1 - 1.7$ GeV is determined almost completely by the weight of the $\hat{A}\{d^* + p\}$ channel of the ^{3}He wave function.

7. CONCLUSION

Our analysis of backward elastic p^3He scattering at energies of 1–2 GeV has revealed three striking effects.

• Of all the mechanisms considered, the dominant contribution comes only from the graph corresponding to sequential pn-pair transfer. The triangle one-pion exchange graph, the pole deuteron-exchange graph, and the loop graphs corresponding to interacting-pair exchange and nonsequential pn-pair transfer contribute at a level several orders of magnitude lower than the dominant mechanism.

• Rescattering in the initial and final states dramatically affects the absolute value and the nature of the angular dependence of the differential cross section. When rescattering is neglected, the theoretical results disagree strongly with the experimental data, and when these effects are included, agreement with experiment is obtained without the introduction of any fitted parameters.

• The cross section depends very strongly on the details of the structure of the ^{3}He nucleus. In particular, when the first channel ($\nu = 1$) in the Faddeev component of the wave function, corresponding to the $\hat{A}\{d^* + p\}$ configuration of the ^{3}He nucleus, is excluded, the differential cross section for elastic p^3He scattering is decreased by 5–6 orders of magnitude.

At energies $T_p \leq 0.9$ GeV the contribution of the ST mechanism turns out to be considerably lower than the experimental data on backward p^3He scattering, owing to the deep minimum in the cross section at $T_p \sim 0.3$ GeV. The dominant contribution at energies $T_p \leq 0.9$ GeV apparently comes from the multiple-scattering mechanisms with antisymmetrized pN amplitudes studied in Refs. 8 and 54.

These results show that attempts to describe backward elastic p^3He scattering by the deuteron-exchange model[10] with phenomenological wave functions are completely unjustified. Going beyond the pole graph of deuteron exchange and also the use of the realistic three-body ^{3}He wave function are of fundamental importance in this problem. It can be expected that the mechanisms of sequential pn- and nn-pair transfer, but not at all deuteron and bineutron transfer, play an analogous rôle in backward elastic α^6Li and α^6He scattering at initial energies ~ 150 MeV. An additional criterion for checking the role of sequential pn-pair transfer in backward elastic p^3He scattering might be provided by measurement of the polarization characteristics of this process. It would be interesting to study the analogous mechanism in backward elastic $p\alpha$ scattering.

The author would like to thank L. D. Blokhintsev, V. G. Neudachin, V. I. Komarov, V. I. Kukulin, and A. V. Lado for many useful discussions of the problems considered here. This study was performed with the partial support of the Russian Fund for Fundamental Research, Grant No. 96-02-17-458.

[1)]Nevertheless, the parentage expansion of the function (94) contains the "excited" state of the nucleon pair {23} with quantum numbers $S = 0$, $T = 1$ with nonzero weight.[56]

[1] P. Berthet *et al.*, Phys. Lett. B **106**, 465 (1981).
[2] P. Bosted, R. E. Arnold, S. Rock *et al.*, Phys. Rev. Lett. **49**, 1380 (1982).
[3] A. K. Kerman and L. S. Kisslinger, Phys. Rev. **180**, 1483 (1969).
[4] L. A. Kondratyuk, F. M. Lev, and L. V. Shevchenko, Yad. Fiz. **33**, 1208 (1981) [Sov. J. Nucl. Phys. **33**, 642 (1981)].
[5] N. S. Craigie and C. Wilkin, Nucl. Phys. B **14**, 477 (1969).
[6] V. M. Kolybasov and N. Ya. Smorodinskaya, Phys. Lett. B **37**, 272 (1971); Yad. Fiz. **17**, 1211 (1973) [Sov. J. Nucl. Phys. **17**, 630 (1973)]; A. Nakamura and L. Satta, Nucl. Phys. A **445**, 706 (1985).
[7] B. Z. Kopeliovich and F. Niedermaier, Zh. Éksp. Teor. Fiz. **87**, 1121 (1984) [Sov. Phys. JETP **60**, 640 (1984)].
[8] M. J. Páez and R. H. Landau, Phys. Rev. C **29**, 2267 (1984).
[9] A. V. Lado and Yu. N. Uzikov, Phys. Lett. B **279**, 16 (1992).
[10] A. P. Kobushkin, in *Proceedings Intern. Conf. DEUTERON-93*, Dubna, 1993, edited by V. K. Lukyanov, p. 71.
[11] M. Levitas and J. V. Noble, Nucl. Phys. A **251**, 385 (1975).
[12] Yu. N. Uzikov, Yad. Fiz. **60**, 1603 (1997) [Phys. At. Nucl. **60**, 1458 (1997)].
[13] G. W. Barry, Phys. Rev. D **7**, 1441 (1973).
[14] H. Lesniak and L. Lesniak, Acta Phys. Pol. B **9**, 419 (1978).
[15] M. S. Abdelmonem and H. S. Sherif, Phys. Rev. C **36**, 1900 (1987).
[16] F. D. Santos, A. M. Eiro, and A. Barosso, Phys. Rev. C **19**, 238 (1979).
[17] D. R. Lehman and B. F. Gibbson, Phys. Rev. C **29**, 1017 (1984).
[18] V. V. Burov *et al.*, Z. Phys. A **306**, 149 (1982).
[19] S. I. Vilen'kaya *et al.*, Zh. Éksp. Teor. Fiz. **60**, 460 (1971) [Sov. Phys. JETP **33**, 247 (1971)].
[20] R. G. Arnold *et al.*, Phys. Rev. Lett. **40**, 1429 (1978).
[21] R. A. Brandenburg, Y. Kim, and A. Tubis, Phys. Rev. C **12**, 1368 (1975).
[22] H. Lesniak, L. Lesniak, and A. Tekou, Nucl. Phys. A **267**, 503 (1976).
[23] M. A. Zhusupov, Yu. N. Uzikov, and G. A. Yuldasheva, Izv. Akad. Nauk Kazakh SSR, Ser. Fiz. No. 6, 69 (1986) [in Russian].
[24] B. L. G. Bakker, L. A. Kondratyuk, and M. V. Terentjev, Nucl. Phys. B **158**, 497 (1979).
[25] S. A. Gurvitz, Phys. Rev. C **22**, 724 (1980).
[26] M. A. Zhusupov and Yu. N. Uzikov, J. Phys. G **7**, 1621 (1981).
[27] Particle Data Group, Report UCRL 20000 NN.1979 (1979).
[28] A. V. Lado and Yu. N. Uzikov, Yad. Fiz. **50**, 1309 (1989) [Sov. J. Nucl. Phys. **50**, 815 (1989)].
[29] M. Igarashi, K. Kudo, and K. Yagi, Phys. Rep. **199**, 1 (1991).
[30] A. V. Lado and Yu. N. Uzikov, Yad. Fiz. **56**, No. 9, 114 (1993) [Phys. At. Nucl. **56**, 1216 (1993)].
[31] A. B. Lado and Yu. N. Uzikov, Izv. Ross. Akad. Nauk, Ser. Fiz. **57**, 122 (1993) [Bull. Russ. Acad. Sci., Phys. Ser.].
[32] L. D. Blokhintsev, A. V. Lado, and Yu. N. Uzikov, Nucl. Phys. A **597**, 487 (1996).
[33] L. D. Blokhintsev and É. Dolinskiĭ, Yad. Fiz. **5**, 797 (1967) [Sov. J. Nucl. Phys. **5**, 565 (1967)].
[34] L. D. Faddeev, Zh. Éksp. Teor. Fiz. **39**, 1459 (1960) [Sov. Phys. JETP **12**, 1014 (1961)].
[35] J. R. Taylor, *Scattering Theory: the Quantum Theory of Nonrelativistic Collisions* (Wiley, New York, 1972) [Russ. transl., Mir, Moscow, 1976].
[36] V. M. Kolybasov, Yad. Fiz. **49**, 412 (1989) [Sov. J. Nucl. Phys. **49**, 256 (1989)].
[37] M. L. Goldberger and K. M. Watson, *Collision Theory* (Wiley, New York, 1964) [Russ. transl., Mir, Moscow, 1967].
[38] L. W. Person and P. Benioff, Nucl. Phys. A **187**, 401 (1972); M. A. Zhusupov and Yu. N. Uzikov, Fiz. Élem. Chastits At. Yadra **18**, 323 (1987) [Sov. J. Part. Nucl. **18**, 136 (1987)].
[39] A. G. Sitenko, Fiz. Élem. Chastits At. Yadra **4**, 547 (1973) [Sov. J. Part. Nucl. **4**, (1973)].
[40] W. Cziz and L. Lesniak, Phys. Lett. B **24**, 227 (1967).
[41] Ch. H. Hajduk, A. M. Green, and M. E. Sainio, Nucl. Phys. A **337**, 13 (1980).
[42] A. G. Baryshnikov, V. B. Belyaev, L. D. Blokhintsev *et al.*, Yad. Fiz. **32**, 369 (1980) [Sov. J. Nucl. Phys. **32**, 191 (1980)].
[43] F. M. Lev, Ann. Phys. (N.Y.) **237**, 355 (1995); Fiz. Élem. Chastits At. Yadra **21**, 1251 (1990) [Sov. J. Part. Nucl. **21**, 534 (1990)]; *Some Problems in the Relativistic Quantum Mechanics of Systems with a Given Number of Degrees of Freedom* [in Russian] (Dubna, 1988).

[44]O. Imambekov, Yu. N. Uzikov, and L. V. Shevchenko, Z. Phys. A **332**, 349 (1989).
[45]A. V. Blinov and I. M. Narodetskiĭ, Yad. Fiz. **36**, 103 (1982) [Sov. J. Nucl. Phys. **36**, 60 (1982)].
[46]E. G. Alt, P. Grassberger, and W. Sandhas, Phys. Rev. C **1**, 85 (1970); A. G. Baryshnikov *et al.*, Nucl. Phys. A **224**, 61 (1974).
[47]P. N. Shen *et al.*, Phys. Rev. C **33**, 1214 (1986).
[48]M. N. Ustinin and V. D. Éfros, Preprint IAÉ-4689/2, Kurchatov Institute, Moscow (1988) [in Russian].
[49]I. Reichstein, D. R. Thompson, and Y. C. Tang, Phys. Rev. C **3**, 2139 (1971); M. LeMere *et al.*, Phys. Rev. C **12**, 1140 (1975).
[50]G. V. Avakov *et al.*, Yad. Fiz. **47**, 1508 (1988) [Sov. J. Nucl. Phys. **47**, 957 (1988)].
[51]Yu. N. Uzikov, Preprint E2-98-112, JINR, Dubna (1998); E-print archive, LANL, nucl-th/9805026; Phys. Rev. C **58** (in press).
[52]R. Dymarz and A. Malecki, Phys. Lett. B **66**, 413 (1977).
[53]B. K. Jain and A. B Santra, Phys. Lett. B **224**, 5 (1990).
[54]D. K. Hasel *et al.*, Phys. Rev. C **34**, 236 (1986).
[55]K. Wildermuth and Y. C. Tang, *A Unified Theory of the Nucleus* (Academic Press, New York, 1977) [Russ. transl., Mir, Moscow, 1980].
[56]V. G. Neudachin and Yu. F. Smirnov, *Nucleon Associations in Light Nuclei* [in Russian] (Nauka, Moscow, 1969).
[57]G. Alberi, L. P. Rosa, and Z. D. Tome, Phys. Rev. Lett. **34**, 503 (1975).

Translated by Patricia A. Millard